

Decomposing past and future: Integrated information decomposition based on shared probability mass exclusions.

Thomas F. Varley^{1,2*}

¹*Department of Psychological and Brain Sciences and*

²*School of Informatics, Computing & Engineering,*

Indiana University, Bloomington, IN 47405

(Dated: March 3, 2022)

A core feature of complex systems is that the interactions between elements in the present causally constrain each-other as the system evolves through time. To fully model all of these interactions (between elements, as well as ensembles of elements), we can decompose the total information flowing from past to future into a set of non-overlapping temporal interactions that describe all the different modes by which information can flow. To achieve this, we propose a novel information-theoretic measure of temporal dependency ($I_{\tau sx}$) based on informative and misinformative local probability mass exclusions. To demonstrate the utility of this framework, we apply the decomposition to spontaneous spiking activity recorded from dissociated neural cultures of rat cerebral cortex to show how different modes of information processing are distributed over the system. Furthermore, being a localizable analysis, we show that $I_{\tau sx}$ can provide insight into the computational structure of single moments. We explore the time-resolved computational structure of neuronal avalanches and find that different types of information atoms have distinct profiles over the course of an avalanche, with the majority of non-trivial information dynamics happening before the first half of the cascade is completed. These analyses allow us to move beyond the historical focus on single measures of dependency such as information transfer or information integration, and explore a panoply of different relationships between elements (and groups of elements) in complex systems.

Keywords: Information theory, information decomposition, excess entropy, synergy, redundancy, neuroscience, criticality, computational dynamics.

I. INTRODUCTION

What does it mean for a complex system to have “structure,” or even to be a “system” at all? Nature abounds with systems: almost every object, when examined closely enough, is actually a composite structure, comprised of many interacting components: the world that we perceive is a dynamic congeries of complex interactions and relationships. It is those relationships that define the nature, and structure of the systems of which they are a part. For a system to have “structure,” its behavior in the future must be some consequence of its behavior in the past. When parts of the system interact, the states of individual elements, or ensembles of elements, constrain their own possible futures, the futures of those components they interact with, and ultimately, the future of the system as a whole. For example, a single neuron embedded in a neuronal network might fire at some time $t - \tau$: that firing, constrains its own future (albeit transiently) due to subsequent hyper-polarization and the refractory period. It also informs on the possible futures of all those post-synaptic neurons to which it was coupled: the probability that they in turn will fire changes after one of their parents fires and so on. In particular cases, the firing of a single neuron (or just a few neurons) may radically constrain the future of the entire brain (for example, if it triggers an epileptic seizure).

The entire scientific endeavour is, in some sense, built on uncovering these dependencies and understanding their specifics. For a complex system \mathbf{X} , comprised of many interacting parts, we can quantify the total degree to which its future can be predicted based on its past with the *excess entropy* [1]:

$$E(\mathbf{X}) = I(\mathbf{X}_{-\infty:t}; \mathbf{X}_{t:\infty}) \quad (1)$$

Where $\mathbf{X}_{-\infty:t}$ corresponds to the joint state of every past instance of time from the first moment up to time t and vice versa for $\mathbf{X}_{t:\infty}$, which corresponds to the infinite future (we adopt the Python-like notation from [2]). In the complete case, accounting for extended periods of past and future makes visible dependencies of varying temporal duration (e.g. distance-related delays in communication networks). In practice, there are practical problems associated with recording infinite data and so the full excess entropy is inaccessible. In the particular case of Markovian systems, however, the situation is considerably easier, as the excess entropy reduces to the mutual information between a moment and time and its immediate past (possibly incorporating a lag of $-\tau$ moments):

$$E'(\mathbf{X}) = I(\mathbf{X}_{-\tau}; \mathbf{X}_t) \quad (2)$$

For example, consider a two element system with Markovian dynamics: $\mathbf{X} = \{X^1, X^2\}$ (following [3] we

* tvarley@indiana.edu

use superscripts to denote indexes and subscripts to denote time). We can compute the lag- τ excess entropy of \mathbf{X} as a whole as:

$$E'(\mathbf{X}) = I(X_{-\tau}^1, X_{-\tau}^2; X_t^1, X_t^2) \quad (3)$$

The excess entropy is an extremely coarse measure, aggregating all of the temporal statistical dependencies, at every scale, within a multivariate system into a single number. For a more “complete” understanding of the dependencies within a system, we would like to be able to decompose it into non-overlapping components that describe how particular elements (and ensembles of elements) constrain each other as the system evolves through time: for example, how does the state of X^1 at time $t - \tau$ constrain its own future? How does it constrain the future of X^2 ? Other, more exotic dependencies are also possible: for example, the joint state of $X_{-\tau}^1$ and $X_{-\tau}^2$ together may constrain the future of just X_t^1 (a phenomena sometimes referred to as “downward causation”, which has been the subject of intense philosophical debate [4, 5]). There may be information about the future of X_t^1 that is redundantly disclosed by both $X_{-\tau}^1$ and $X_{-\tau}^2$ considered individually, and so on. How can we untangle all of these different dependencies?

One possible path forward comes from the field of information decomposition. Classically, information decomposition concerned itself with the question of how to best understand how different ensembles of *predictor* variables collectively disclose information about a single *target* variable [6, 7]. Since the original introduction of the *partial information decomposition* (PID) framework by Williams and Beer in 2010, researchers in complex systems science, information theory, and theoretical neuroscience have collectively worked to deepen our understanding of multivariate information and higher-order dependencies. Recently, Mediano, Rosas, and other introduced a multi-target information decomposition (the *integrated information decomposition* (Φ ID)) [3, 8, 9] which extends the original framework to multiple targets, enabling a full decomposition of the excess entropy. Despite being a considerable leap forward in our understanding of multivariate, temporal information, like the original PID, the Φ ID lacks a crucial element required for applications to real data: an operational definition of *multivariate redundancy*.

In this work, we propose such a redundancy function, which we term $I_{\tau sx}$. Based on a recent single-target measure introduced by Makkeh et al., [10] our proposed measure generalizes the classic Shannon mutual information function to ensembles of multiple interacting elements that may redundantly disclose information about each other. We begin by reviewing the classic, single-target PID, before generalizing to the Φ ID. We then introduce the $I_{\tau sx}$ measure, and demonstrate its application in three constructed Markovian systems designed to display distinct dynamical differences, and finally empirical, neuronal spiking data recorded from dissociated cultures of

mouse hippocampal cortex [11, 12]. We conclude by discussing the strengths and limitations of our measure, and the Φ ID framework itself.

A. Partial Information Decomposition

1. Intuition & the Bivariate Case

Consider the the simple case where we have two *predictor* variables (X^1 and X^2) that jointly disclose information about a target variable Y . Basic information theory gives us the tools to asses how each X individually informs on Y (the marginal mutual informations, e.g. $I(X^1; Y)$ etc), and how the joint state of both X^1 and X^2 together inform on Y : $I(X^1, X^2; Y)$. The relationship between the marginal and joint mutual informations is not always straight-forward, however: the sum of both marginal mutual informations can be *greater than* or *less than* the joint mutual information in various contexts. If $I(X^1; Y) + I(X^2; Y) > I(X^1, X^2; Y)$, then there must be some information about Y that is *redundantly* present in both X^1 and X^2 individually, and so when the two marginal mutual informations are summed, that redundant information is “double counted.” Conversely, if $I(X^1; Y) + I(X^2; Y) < I(X^1, X^2; Y)$, then there is information about Y in the joint state of X^1 and X^2 that is only accessible when the two are considered together and not accessible by looking at any individual X . These comparisons of “wholes” to “parts” are only rough heuristics, however, as redundant and synergistic information can co-exist in a set of predictor variables [6]: the direction of the inequality only indicates whether synergistic or redundant information *dominates* the interaction.

The seminal contribution of Williams and Beer was to provide a mathematical framework that allowed for a complete decomposition of the joint mutual information into non-overlapping, additive “atoms” of information:

$$\begin{aligned} I(X^1, X^2; Y) = & Red(X^1, X^2; Y) \quad (4) \\ & + Unq(X^1; Y|X^2) \\ & + Unq(X^2; Y|X^1) \\ & + Syn(X^1, X^2; Y) \end{aligned}$$

where $Red(X^1, X^2; Y)$ is the redundant information about Y that could be learned by observing *either* X^1 or X^2 individually, $Unq(X^1; Y|X^2)$ is the information about Y that is *uniquely* disclosed by X^1 (in the context of X^2 , a vice versa for the other unique atom), and $Syn(X^1, X^2; Y)$ is the synergistic information about Y that can only be learned by observing X^1 and X^2 simultaneously. Furthermore, we can break down the “marginal mutual informations” with the same atomic components:

$$\begin{aligned} I(X^1; Y) &= Red(X^1, X^2; Y) + Unq(X^1; Y|X^2) \quad (5) \\ I(X^2; Y) &= Red(X^1, X^2; Y) + Unq(X^2; Y|X^2) \end{aligned}$$

The result (in the case of two predictor variables) is an under-determined system with three known values (the three mutual information terms) and four unknown values (each of the partial-information atoms). If any one atom can be determined, then we get the remaining “three for free.” Classical information theory does not provide any specific functions for any of these terms [13], and consequently their development is an area of active, and on-going, research. It is most common to begin by defining a redundancy function [6], although approaches based on defining unique [14, 15] and synergistic information [16, 17] have also been proposed. Unfortunately, if the number of sources is greater than two, the resulting decompositions of the joint and marginal mutual informations are not so constrained and more advanced mathematical machinery is required to decompose the joint mutual information.

2. The Partial Information Lattice & Möbius Inversion

For a collection of N predictor variables $\mathbf{X} = \{X^1, \dots, X^N\}$ jointly informing on a single target Y , we are interested in understanding how every $X_i \in \mathbf{X}$ (and ensembles of X s joint by the logical conjunction) disclose information about the target. This requires understanding all the ways that the elements of \mathbf{X} can redundantly, uniquely, and synergistically share information. Williams and Beer showed that, given an measure of redundant (or shared) information between some collection of sources and the target (denoted $I_{\cap}(\cdot; Y)$ here), the “atomic” components of the joint mutual information are constrained into a partially ordered set called the *partial information lattice*. The derivation of the lattice will be briefly described below, but see Gutknecht et al., for a more complete discussion [7].

We begin by defining the set of *sources* that may disclose information about Y . This is given by the set of all subsets of \mathbf{X} (excluding the empty set, denoted as $\mathcal{P}_1(\mathbf{X})$). Every (potentially multivariate) source can be thought of as an aggregated macro-variable, whose state is defined by the logical-AND operator over all of its constituent elements. For example, if our predictor variables are X^1 , X^2 and X^3 , then the collections of sources are:

$$\left\{ \begin{array}{l} \{X^1\}, \{X^2\}, \{X^3\}, \\ \{X^1 \wedge X^2\}, \{X^1 \wedge X^3\}, \{X^2 \wedge X^3\}, \\ \{X^1 \wedge X^2 \wedge X^3\} \end{array} \right\} \quad (6)$$

For some (potentially overlapping) collection of sources, $\mathbf{A}^1, \dots, \mathbf{A}^k$, the redundancy function $I_{\cap}(\mathbf{A}^1, \dots, \mathbf{A}^k; Y)$ quantifies the information about Y that can be learned by observing $\mathbf{A}^1 \vee \dots \vee \mathbf{A}^k$. The domain of the $I_{\cap}(\cdot; Y)$ is given by the set of all collections of sources such that no source is a subset of any other:

$$\mathcal{A} = \{\alpha \in \mathcal{P}_1(\mathcal{P}_1(\mathbf{X})) : \forall \mathbf{A}^i, \mathbf{A}^j \in \alpha, \mathbf{A}^i \not\subseteq \mathbf{A}^j\} \quad (7)$$

This restriction means that that \mathcal{A} is also partially ordered:

$$\forall \alpha, \beta \in \mathcal{A}, \alpha \preceq \beta \Leftrightarrow \forall \mathbf{B} \in \beta, \exists \mathbf{A} \in \alpha \text{ s.t. } \mathbf{A} \subseteq \mathbf{B} \quad (8)$$

The resulting lattice $\langle \mathcal{A}, \preceq \rangle$ provides the scaffolding on which the full PID may be constructed. Every $\alpha \in \mathcal{A}$ corresponds to a vertex on the lattice, and the ordering reveals a structure of increasingly synergistic information-sharing relationships. For a visualization of the partial information lattices for sets of two and three predictor variables, see Figure IA 2.

With the structure of the partial information lattice set and our as-yet-undefined redundancy function in place $I_{\cap}(\cdot; Y)$, we can solve the PID for every $\alpha \in \mathcal{A}$ using a Möbius inversion:

$$\Pi(\alpha) = I_{\cap}(\mathbf{A}^1, \dots, \mathbf{A}^{|\alpha|}; Y) - \sum_{\beta \prec \alpha} \Pi(\beta) \quad (9)$$

By recursively defining the value of particular partial information atoms as the difference between the redundancy information disclosed by a particular set of sources and the sum of all atoms lower on the lattice, we can finally decompose the joint mutual information between an arbitrary number of predictor variables and a single target.

$$I(\mathbf{X}; Y) = \sum_{i=1}^{|\mathcal{A}|} \alpha_i \quad (10)$$

B. Integrated Information Decomposition

With the basic PID defined, it is possible to do a partial examination of the excess entropy. For example, Varley and Hoel [18] decomposed the joint mutual information between all elements at time $t - \tau$ and the joint state of the whole system at time t : $I(X_{-\tau}^1, \dots, X_{-\tau}^N; \mathbf{X}_t)$. This method provides insights into how the states of particular elements (and ensembles of elements) collectively constrain the future of the whole system, but provides no insights into how parts of the system constrain each-other, as the future state is aggregated into a single, unitary “whole.”

To address this limitation, Mediano et al., [3, 8] recently introduced a generalization of the PID that allows the decomposition of multiple sources onto multiple targets. Called the *integrated information decomposition* (Φ ID), this decomposition allows for a complete decomposition of the excess entropy.

The integrated information decomposition begins by defining a *product lattice* $\mathcal{A}^2 = \mathcal{A} \times \mathcal{A}$ (where \mathcal{A} is the single-target redundancy lattice derived above), for which each vertex in \mathcal{A}^2 is defined by an ordered pair $\alpha \rightarrow \beta$, with $\alpha, \beta \in \mathcal{A}$. In the case of a temporal process,

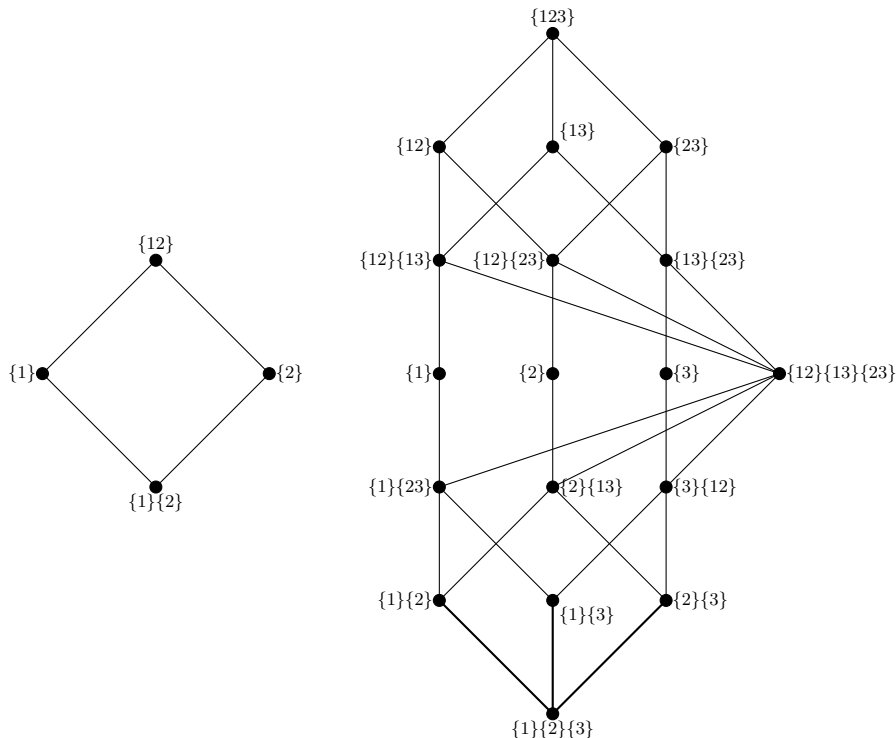


FIG. 1. **Single target partial information lattices.** Examples of partial information lattices for the two simplest possible systems of multiple sources predicting a single target. On the left is the lattice for two predictor variables, and on the right is the lattice for three predictor variables. Following the notation introduced by Williams and Beer [6], sources are denoted just by index: for example $\{1\}\{2\}$ is the information redundantly disclosed by X^1 or X^2 , $\{1\}\{23\}$ is the information disclosed by X^1 or (X^2 and X^3), etc.

α refers to a particular collection of sources observed at time $t - \tau$ that disclose information about β , a collection of sources observed at time t .

As with the single-target partial information lattice, the product lattice is a partially ordered set, with:

$$\alpha \rightarrow \beta \preceq \alpha' \rightarrow \beta' \Leftrightarrow \alpha \preceq \alpha', \beta \preceq \beta' \quad (11)$$

the integrated information lattice can be similarly solved via Möbius inversion, given a suitable temporal redundancy function $I_{\cap}^{\alpha \rightarrow \beta}$. For a visualization of the integrated information lattice for the case of two sources and two targets, see Figure 2.

1. Interpreting Φ ID Atoms

The standard PID atoms are reasonably easy to interpret in terms of logical conjunctions of predictors (sources) and logical disjunctions (redundant information about a single target shared between sources). In the case of the Φ ID, the left-hand side of the integrated information atom remains the same (collections of sources that redundantly disclose information), but there is no longer a consistent target. Rather, there are again collections of

sources that have their own redundant information sharing patterns. What, then, are they disclosing information *about*? We will discuss the answer in formal detail below, however, one proposed intuition is in the form of information dynamics. Information dynamics proposes to break the different “modes” of information flow in complex systems down into discrete “types of computation” or “processing” [19]. Mediano et al. [3, 8], proposed the following intuitive taxonomy of integrated information atoms on the two-element lattice:

Information Storage: Information present in a particular configuration at time $t - \tau$ that remains in the same configuration at time t . In the case of the two-element system, these are: $\{1\}\{2\} \rightarrow \{1\}\{2\}$, $\{1\} \rightarrow \{1\}$, $\{2\} \rightarrow \{2\}$, and $\{12\} \rightarrow \{12\}$.

Causal Decoupling: The double-synergy term $\{12\} \rightarrow \{12\}$ has been given particular focus as a possible formal definition of “emergent dynamics” [3, 9], as it refers to information that is present in the whole, but none of the parts.

Information Transfer: Information present in a single element that “moves” to another single element: $\{1\} \rightarrow \{2\}$ and $\{2\} \rightarrow \{1\}$. Not to be

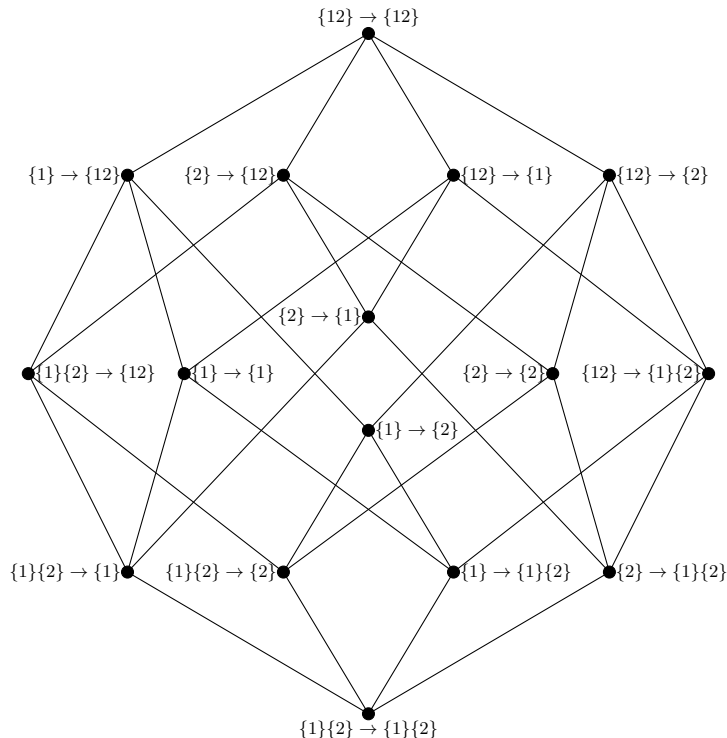


FIG. 2. **The integration information lattice.** The integrated information lattice for a system $\mathbf{X} = \{X^1, X^2\}$. Every vertex of the lattice corresponds to a specific “conversion of information” that information in one mode at time $t - \tau$ can be transformed into at time t . For example, $\{1\}\{2\} \rightarrow \{1\}$ corresponds to information that is *redundantly* disclosed by X^1 and X^2 at time $t - \tau$ that is then only uniquely disclosed by X^1 at time t .

confused with the transfer entropy [20], which typically involves extended histories and itself conflates unique and synergistic modes of information sharing [21].

Information Erasure: Information that is initially present redundantly over multiple elements that is erased from one of the two: $\{1\}\{2\} \rightarrow \{1\}$ and $\{1\}\{2\} \rightarrow \{2\}$.

Information Copying: Information that is initially present only a single element that is “duplicated” to be redundantly present in multiple elements. $\{1\} \rightarrow \{1\}\{2\}$ and $\{2\} \rightarrow \{1\}\{2\}$.

“Upward Causation”: A somewhat less well-defined idea: when the state of single elements constrains the future state of the entire ensemble. $\{1\}\{2\} \rightarrow \{12\}$, $\{1\} \rightarrow \{1\}\{2\}$, and $\{2\} \rightarrow \{1\}\{2\}$.

“Downward Causation”: A philosophically controversial concept, downward causation occurs when the synergistic joint state of the “whole” constrains the future of the individual parts. $\{12\} \rightarrow \{1\}\{2\}$, $\{12\} \rightarrow \{1\}$, and $\{12\} \rightarrow \{2\}$

This intriguing taxonomy has only begun to be explored (for example see [22, 23] for intriguing results re-

lated to macro-scale brain dynamics), and a rigorous formal understanding of the relevant mathematics may help deepen our understanding of these various (and in some cases, philosophically significant) phenomena.

II. SHARED EXCLUSIONS & (TEMPORAL) REDUNDANCY

A peculiar quirk of the PID and its derivatives is that, while it reveals the “structure” of multivariate information, it doesn’t provide a direct means of calculating the specific values: it assumes the existence of a well-behaved redundancy measure and builds from there. Since the initial introduction by Williams and Beer, the number of different redundancy functions has proliferated (see [10, 13, 24–33]), although to date, no measure has achieved universal acceptance or satisfies every desiderata.

Being much newer, there has been less work on double redundancy functions: to date, only two have been used: a temporal minimum mutual information analysis [22, 23, 34], and a generalization of the common change in surprisal measure [3]. While both analyses are informative, there is still room for deeper insights into the exact nature of temporal redundancy and how information

conversion occurs between ensembles of variables. In this work, we generalize a recent redundancy function, the I_{sx} measure first proposed by Makkeh et al., [10], to account for multiple targets which we term $I_{\tau sx}$. We selected I_{sx} as our starting point for two reasons: the first is that it illuminates an elegant connection between multivariate information sharing and formal logic, and second, because it does not require arbitrary thresholds (as in the case of I_{ccs} [30]) nor non-differentiable min/max functions (as in I_{mmi} [28] and the closely related I_{\pm} [31]). Below, we introduce the basics of local information theory (a key prerequisite for defining I_{sx}), before defining the redundancy function for single targets, and ultimately generalizing to multi-target information.

A. Local Information Theory

Thus far, we have been using the standard interpretation of mutual information as an average value over some distribution of configurations;

$$I(X; Y) := \mathbb{E}_{X, Y} \left[\log_2 \frac{P(y|x)}{P(y)} \right] \quad (12)$$

For any *specific* configuration, we define the *local mutual information* as:

$$i(x; y) := \log_2 \frac{P(y|x)}{P(y)} \quad (13)$$

Unlike the expected mutual information, the local mutual information can be either positive or negative depending on whether $P(x|y)$ or $P(x)$ is the greater term. While the local mutual information is well-explored and has been previously used extensively to characterize “computation” in complex systems [19], it is only recently that a novel interpretive framework has emerged based on exclusions of probability mass. Finn and Lizier [35] showed that the sign and value of the local mutual information $i(x; y)$ can be understood as a function of the amount of probability mass from $P(X, Y)$ that is “ruled out” upon observing that $X = x$ and $Y = y$. For a very simple example, consider a system where one player rolls a fair die and another has to guess the value. Initially, the guesser is maximally uncertain, as all six outcomes are equiprobable. However, if they learn that the the number rolled was *even*, then they have *gained* information proportional to the total probability mass of all excluded possible outcomes. Formally, we can re-write the local mutual information in terms of probability mass exclusions as:

$$i(x; y) = \log_2 \frac{P(y) - P(y \cap \bar{x})}{P(1 - \bar{x})} - \log_2 P(y) \quad (14)$$

In this relationship, if y is comparatively *more* likely after accounting for x , then $i(x; y) > 0$, and if it is less likely, then the value is negative.

B. Single-Target Redundancy Based on Shared Exclusions (I_{sx})

Consider a set of (potentially overlapping, potentially multivariate) sources $\mathbf{a}^1, \dots, \mathbf{a}^k$ that collectively disclose information about a target y . We define the information redundantly shared between them as a function the probability mass of $P(Y)$ that would be excluded regardless of whether we observed $\mathbf{a}_1 \vee \dots \vee \mathbf{a}^k$:

$$i_{sx}(\mathbf{a}^1, \dots, \mathbf{a}^k; y) := \log_2 \frac{P(y) - P(y \cap (\bar{\mathbf{a}}^1 \cap \dots \cap \bar{\mathbf{a}}^k))}{1 - P(\bar{\mathbf{a}}^1 \cap \dots \cap \bar{\mathbf{a}}^k)} - \log_2 P(y) \quad (15)$$

For the special case of only one source, it is clear that $i_{sx}(\mathbf{a}; y) = i(\mathbf{a}; y)$, which is itself just a regular joint mutual information: $i(x^{\mathbf{a}^1}, \dots, x^{\mathbf{a}^{|\mathbf{a}|}}; y)$. In this sense, we can understand i_{sx} as generalizing the Shannon mutual information to account for ensembles of multiple sources that redundantly share information about y [7].

Like the standard local mutual information i_{sx} can return both positive and negative values (corresponding to informative and misinformative probability mass exclusions respectively). These two types of exclusion can be quantified by further decomposing i_{sx} into two components:

$$i_{sx}^+(\mathbf{a}^1, \dots, \mathbf{a}^k; y) := \log_2 \frac{1}{P(\mathbf{a}^1 \cup \dots \cup \mathbf{a}^k)} \quad (16)$$

$$i_{sx}^-(\mathbf{a}^1, \dots, \mathbf{a}^k; y) := \log_2 \frac{P(y)}{P(y \cap (\mathbf{a}^1 \cup \dots \cup \mathbf{a}^k))} \quad (17)$$

$$i_{sx}(\mathbf{a}^1, \dots, \mathbf{a}^k; y) = i_{sx}^+(\mathbf{a}^1, \dots, \mathbf{a}^k; y) - i_{sx}^-(\mathbf{a}^1, \dots, \mathbf{a}^k; y) \quad (18)$$

In the context of a single-target PID, i_{sx}^+ and i_{sx}^- are provably non-negative and satisfy the original desiderata proposed by Williams and Beer. The local redundant information measures can be aggregated into expected measures over the distribution of configurations in the same way as mutual information:

$$I_{sx} = \mathbb{E}_{\mathbf{A}^1, \dots, \mathbf{A}^k, Y} [i_{sx}(\mathbf{a}^1, \dots, \mathbf{a}^k; y)] \quad (19)$$

and likewise for the informative and misinformative functions.

C. Multi-Target Temporal Redundancy Based on Shared Exclusions ($I_{\tau sx}$)

We now have all the required machinery to introduce our local measure of temporal information decomposition: $I_{\tau sx}$. In the original i_{sx} measure, the mutual information is understood as the relative increase or decrease

in the probability $P(Y = y)$ after observing the configuration of some ensemble of sources. In $I_{\tau sx}$, the probability of the single target is replaced with the probability of observing $\mathbf{b}^1 \vee \dots \vee \mathbf{b}^m$:

$$I_{\tau sx}(\mathbf{a}^1, \dots, \mathbf{a}^k; \mathbf{b}^1, \dots, \mathbf{b}^m) := \log_2 \frac{P(\mathbf{b}^1 \cup \dots \cup \mathbf{b}^m) - P((\mathbf{b}^1 \cup \dots \cup \mathbf{b}^m) \cap (\bar{\mathbf{a}}^1 \cap \dots \cap \bar{\mathbf{a}}^k))}{1 - P(\bar{\mathbf{a}}^1 \cap \dots \cap \bar{\mathbf{a}}^k)} - \log_2 P(\mathbf{b}^1 \cup \dots \cup \mathbf{b}^m) \quad (20)$$

From here forward, we will denote ensembles of sources with α , β , etc, for the purposes of notation compactness.

In the special case of single sources ($\alpha = \{\mathbf{a}\}$, $\beta = \{\mathbf{b}\}$), it is clear that $I_{\tau sx}(\mathbf{a}; \mathbf{b}) = i(\mathbf{a}; \mathbf{b})$ and so that $I_{\tau sx}$ completes the generalization of local mutual information begun by i_{sx} : $I_{\tau sx}$ is a full generalization of the mutual information to multiple sets of redundant sources and multiple sets of redundant targets.

We can now return to the question posed in Section IB 1: how does one interpret a partial information atom like $\Pi(\{1\}\{2\} \rightarrow \{1\}\{2\})$? Seen through the lens of probability mass exclusions the answer becomes clear. For an evolving system of two elements, there are some configurations of joint pasts and futures that are consistent with observing either x_t^1 OR x_t^2 in the future. If we then exclude all the configurations that are **not** consistent with $x_{-\tau}^1$ OR $x_{-\tau}^2$, we exclude some of those future configurations. The relative change in probability mass determines the value of $I_{\tau sx}$.

The $I_{\tau sx}$ function inherits the same informative and misinformative decompositions from i_{sx} , however the structure of the double redundancy lattice leads to unexpected consequences:

$$I_{\tau sx}^+(\alpha \rightarrow \beta) := \log_2 \frac{1}{P(\mathbf{a}^1 \cup \dots \cup \mathbf{a}^k)} \quad (21)$$

$$I_{\tau sx}^-(\alpha \rightarrow \beta) := \log_2 \frac{P(\mathbf{b}^1 \cup \dots \cup \mathbf{b}^m)}{P((\mathbf{b}^1 \cup \dots \cup \mathbf{b}^m) \cap (\mathbf{a}^1 \cup \dots \cup \mathbf{a}^k))} \quad (22)$$

$$I_{\tau sx}(\alpha \rightarrow \beta) = I_{\tau sx}^+(\alpha \rightarrow \beta) - I_{\tau sx}^-(\alpha \rightarrow \beta) \quad (23)$$

The informative component, $I_{\tau sx}^+$ is identical to i_{sx}^+ , and so inherits all of its properties, including independence from the future configurations and non-negativity. However, since the same α can appear multiple times on the integrated information lattice (e.g. $\{12\} \rightarrow \{1\}$ and $\{12\} \rightarrow \{12\}$ are both valid atoms), $I_{\tau sx}^+(\alpha \rightarrow \beta)$ will only be non-zero *the first time a particular α appears in the lattice*. For example, the atom $\{1\}\{2\} \rightarrow \{1\}\{2\}$ is the only time that any $I_{\tau sx}^+(\{1\}\{2\} \rightarrow \beta) > 0$. $I_{\tau sx}^-(\alpha \rightarrow \beta)$ is similarly non-negative, although the resulting atoms after performing Möbius inversion are not guaranteed to be. It is not uncommon to see $\Pi^+(\alpha \rightarrow \beta) = 0$, $\Pi^-(\alpha \rightarrow \beta) < 0$, resulting in an overall $\Pi(\alpha \rightarrow \beta) > 0$.

Finally, as with i_{sx} , expected values over the distribution of configurations can be easily computed in the usual way.

III. RESULTS

In this paper, we have proposed a novel function of multi-target redundancy to be used as the foundation of an integrated information decomposition [3, 8]. Based on the logic of information as exclusions of possible configurations [35], our proposed measure, $I_{\tau sx}$, generalizes the single-target redundancy measure first proposed by Makkeh et al., to enable the full decomposition of the excess entropy intrinsic to discrete dynamical processes. To demonstrate the measure in action, in the context of the Φ ID, we will now explore some applications: the first three will be constructed systems designed to display markedly different dynamics (disintegrated, integrated, and heterogeneous) to illustrate how different “types” of integration can be revealed by the decomposition. We will then examine spiking data from dissociated cultures made from rat brain tissue to demonstrate the insights that can be gained from both the expected, and local, integrated information decompositions.

A. Synthetic Systems

Each of the three synthetic system is comprised of two, binary, elements that evolve through times according to different Markovian state-transition networks (visualized in Fig. 3). Prior work on such simple, Boolean network systems has shown that the space of even very small systems has a surprisingly rich distributions of redundant, unique, and synergistic effective information atoms [18]. Despite the extreme simplicity of the synthetic systems under study here, we can see how $I_{\tau sx}$ can reveal markedly different dynamic regimes.

1. Disintegrated System

The first system, \mathbf{S}^D is a “disintegrated” system, in that each of the two dynamic elements is disconnected from the other: both predict *their own* futures with total determinism (the pattern is an oscillation $1 \rightarrow 0 \rightarrow 1 \rightarrow \dots$), however there is no integration. Consequently, the excess entropy $I(\mathbf{S}_{t-1}^D; \mathbf{S}_t^D) = 2$ bit, and both individual excess entropies are each 1 bit: the “whole” is trivially reducible to the sum of its parts, since there’s no actual interaction between elements. For a visualization of the state-transition matrix, see Figure 3, left.

Decomposing the excess entropy using $I_{\tau sx}$ reveals several interesting relationships (for the full decomposition, see Table I). As expected, the strongest information atoms are the element-wise information “storage” atoms: $\{1\} \rightarrow \{1\}$ and $\{2\} \rightarrow \{2\}$ while the two pairwise

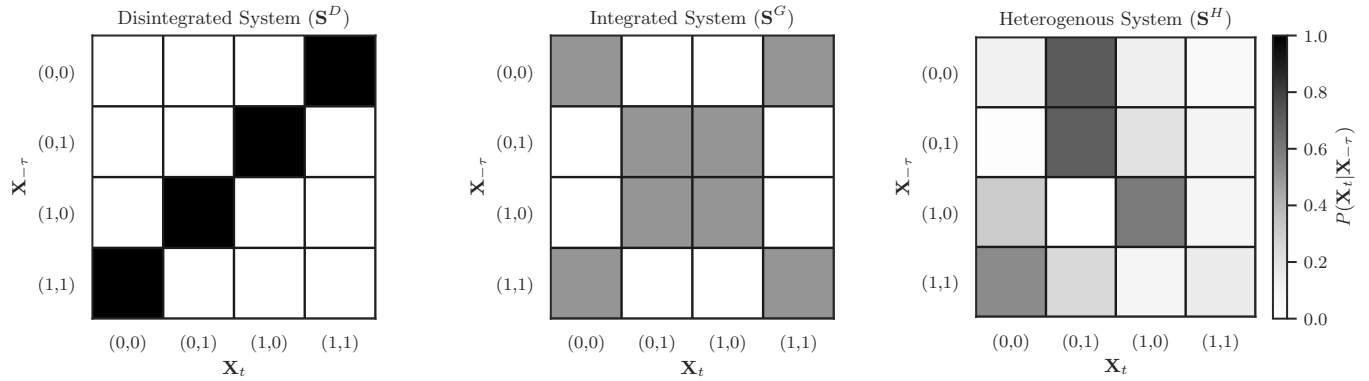


FIG. 3. **Transition probability matrices for simple Boolean network systems.** On the left, we have the disintegrated system, where $E(\mathbf{X}) = E(X^1) + E(X^2) = 2\text{bit}$ (i.e. the whole is equal to the sum of the parts). In the middle, we have the highly integrated system, where $E(\mathbf{X}) = 1$ bit and both $E(X^i) = 0$ bit (i.e. the whole is greater than the sum of it's parts). On the right, we have a random system, combining a heterogenous mixture of integrated and segregated dynamics.

$\alpha \rightarrow \beta$	Disintegrated	Integrated	Heterogeneous
$\{1\}\{2\} \rightarrow \{1\}\{2\}$	0.415	0.152	-0.021
$\{1\}\{2\} \rightarrow \{1\}$	0.0	-0.152	-0.006
$\{1\}\{2\} \rightarrow \{2\}$	0.0	-0.152	0.099
$\{1\} \rightarrow \{1\}\{2\}$	0.0	-0.152	0.008
$\{2\} \rightarrow \{1\}\{2\}$	0.0	-0.152	-0.005
$\{1\} \rightarrow \{2\}$	-0.415	0.152	0.077
$\{2\} \rightarrow \{1\}$	-0.415	0.152	0.055
$\{1\} \rightarrow \{1\}$	0.585	0.152	0.037
$\{2\} \rightarrow \{2\}$	0.585	0.152	-0.072
$\{1\}\{2\} \rightarrow \{12\}$	0.0	-0.433	0.021
$\{12\} \rightarrow \{1\}\{2\}$	0.0	-0.433	0.049
$\{1\} \rightarrow \{12\}$	0.415	0.433	0.032
$\{2\} \rightarrow \{12\}$	0.415	0.433	0.005
$\{12\} \rightarrow \{1\}$	0.415	0.433	-0.008
$\{12\} \rightarrow \{2\}$	0.415	0.433	0.075
$\{12\} \rightarrow \{12\}$	-0.415	-0.018	0.078

TABLE I. **Table of integrated information atoms.** For each of the three Boolean systems, we did the full integrated information decomposition, resulting in sixteen distinct Φ I atoms. The distinct global dynamics are reflected in the varying distributions of informative and misinformative information modes. We note that time-reversible systems (i.e. those where the probability of transitioning from state i to state j is the same as the reverse transition) have a more constrained and symmetrical structure than the heterogeneous system. Whether this is a universal fact about reversible versus irreversible dynamics remains an intriguing topic for future research.

“transfer” atoms are strongly negative (consistent with the notion of the system as a disintegrated structure. Almost all atoms involving redundant information are 0 bit (although the double-redundancy atom is greater than zero. Curiously, there are more positive interactions between individual elements and higher-order synergistic joint-states than anticipated (e.g. $\{1\} \rightarrow \{12\} > 0$ bit). While initially counter-intuitive, we propose that this can be understood when considering the particular local dynamics. Knowing that $\mathbf{S}_{-\tau}^{D1} = 1$ immediately rules out any possible joint future state for \mathbf{S}_t^D where $\mathbf{S}^{D1} = 1$, regardless of whether $\mathbf{S}_{-\tau}^{D2} = 0$ or 1. These results highlight how the space of higher-order interactions can be

counter intuitive and require a fine-grained analysis than a simple scalar measure of “integration.”

2. Integrated System

The second system, \mathbf{S}^G is an “integrated” system, in that there the whole system has 1 bit of excess entropy, but both elements have individual excess entropies of 0 bit. This is accomplished using a parity check function: at every time step, the parity of the system is preserved, but the individual assignments are done randomly. For example, if $\mathbf{S}_{-\tau}^G = (1, 0)$, then \mathbf{S}_t^G could equal $(0, 1)$ or

(1, 0) with equal probability (but never (0, 0) or (1, 1)). For a visualization of the state-transition matrix, see Figure 3, center.

Unlike the disintegrated system, \mathbf{S}^G had no integrated information atoms equal to 0 bit, and only three unique values. With the exception of the $\{1\}\{2\} \rightarrow \{1\}\{2\}$ atom (which was positive), every other atom involving a redundant source was negative, which is consistent with the randomizing component of the updating step. Curiously, the top of the lattice (“causal decoupling”, $\{12\} \rightarrow \{12\}$) was also negative, although the absolute value was low. This was a surprise, as we would have expected such a system to have most, or all, of its temporal information flow in the most synergistic mode. More appropriately, the largest positive values were all in atoms that had a synergy component and a unique component, which is consistent with the overall synergistic dynamic and lack of lower-level dependencies. Like the disintegrated system, the integrated system is non-ergodic, so not every state each reachable from every other state - the extent to which properties such as ergodicity, system size, etc, influence the distribution of integrated information atoms remains an area of further study.

3. Heterogeneous System

The final system was one with heterogeneous transitions, with probabilities drawn from a Gaussian distribution $\mathcal{N}(0, 1)$ (for details, see Varley & Hoel [18]). In contrast to the prior two systems, this system, \mathbf{S}^H does not have an *a priori* fixed “type” of dynamic and was expected to display multiple types of information conversion. From the outset, we anticipated evidence of synergistic dynamics, as the excess entropy of the whole system was 0.422 bit, while each of the two elements had individual temporal mutual informations of 0.017 bit and 0.001 bit respectively, indicating a dynamic where the whole is much more predictive than the sum of its parts. For a visualization of the state-transition matrix, see Figure 3, right.

Consistent with expectations, \mathbf{S}^H did not have the same regularity of information dynamics displayed by \mathbf{S}^D and \mathbf{S}^G : for example, the atom $\{1\}\{2\} \rightarrow \{1\}$ was negative, indicating a misinformative relationship, while $\{1\}\{2\} \rightarrow \{2\}$ was positive and had a greater absolute value. Similarly, the conversion from redundant to synergistic information and vice versa both has opposite signs, suggesting that this system simultaneously displays informative “downward causation”, but misinformative “upward causation”. In totality, there were more informative integrated information atoms than misinformative ones (a ratio of 11 to 5), showing that, despite the overall strongly synergistic nature of the system, unique information transfer and redundant information dynamics all co-existed together. This is consistent with previous work that found that these kinds of modified-Gaussian systems can display a wide range of information dynam-

ics, at multiple scales [18].

B. Dissociated Neural Culture Data

To demonstrate how decomposition of the excess entropy using $I_{\tau_{sx}}$ might be applied to empirical data, we analyzed 31 dissociated cultures of rat hippocampal cortex. These preparations were made by resecting slices of embryonic rat cortex, and then culturing them to produce networks of living neuronal tissue [11]. After preparation of the cultures and a period of maturation, spontaneous spiking activity was then recorded on a 60 electrode array and spike-sorted to produce a time series of spikes for each putative neuron (for details, see the original manuscript presenting these data [12] and the Materials & Methods Section).

Dissociated and organotypic cultures have been a highly productive model system for research into information dynamics and “computation” in biological systems: for example, see studies of the relationship between criticality and information-theoretic complexity [12, 36], network structure and synergy [37–39], changes to computational structure during maturation and development [40–42], and the topology of effective networks [43–45]. In many respects, they are a natural fit for these kinds of information theoretic analyses: neuronal activity is naturally discrete (in the form of action potentials which can be represented with binary states), the neuron is a well-defined “unit” (a single cell), and the communication channels between units is well-understood at the mechanistic level (neurons communicate over synapses via the release of neurotransmitters), as are the general causal effects of interaction (neurons can be inhibitory or excitatory, a relationship easily expressible in terms of Bayesian prior and posterior probabilities [46]).

In this study, we demonstrate the utility of $I_{\tau_{sx}}$ as both an expected and localizable measure of information-sharing by examining the pairwise relationships between neurons. Our particular focus is on avalanches of high-firing activity, which are typical of neural systems and systems poised near a critical phase transition in general. While the question of criticality in the brain is a complex question (for review, see [47, 48], and for a dissenting view, see [49]), it is an empirical fact that spontaneous activity in cortical networks displays avalanche dynamics of widely varying lengths (typically modeled as following a power-law, or other heavy-tailed distribution [50]). While the existence of such avalanches is extremely well-documented, and their genesis the subject of intensive modeling work, it is still unclear what, if any, role they play in cortical computations. Varley et al., hypothesized that they may play an integrative role after finding that loss of consciousness via the anaesthetic propofol caused pronounced collapse of large-scale avalanche structure [51], however, such hypotheses remain highly speculative in the absence of a formal framework for understanding localizable computation. We propose that

the Φ ID framework, coupled with the intrinsically local nature of $I_{\tau sx}$ solves that problem.

1. Distributions of Average Φ ID Atoms

For each of the 31 cultures, we calculated the lag-1 excess entropy for every pair of nodes in the network (restricting our analysis to consecutive bins within avalanches, as in [42]). If the expected excess entropy was significant at $\alpha = 10^{-6}$, (Bonferroni corrected), we went on to do the full integrated information decomposition. The result is, for every culture, across all pairs of nodes with significant excess entropy, we can compute sixteen distinct pairwise “integrated information matrices” (for visualization see Fig. 4). For these expected values, we normalized each one by dividing it by its associated excess entropy to control for the variability in the overall amount of temporal information:

To explore the overall distribution of normalized information atoms, we aggregated over all cultures to create histograms of the various Φ ID components (Fig. 5). We found that the element-level information storage atoms ($\{x\} \rightarrow \{x\}$) had the overall highest average normalized value (0.417 ± 0.422), followed by the element-level information transfer atoms ($\{x\} \rightarrow \{y\}$, 0.097 ± 0.195). These results are consistent with our initial expectations: individual neurons are known to have a strong individual temporal dependence [53, 54], likely reflecting the refractory period following an action potential). Similarly, the high element-wise information transfer is consistent with the basic mode of communication between neurons being pairwise synaptic signaling. The other modes of information conversion, however, remain more mysterious: for example, the information copy and information erasure atoms ($\{x\} \rightarrow \{1\}\{2\}$ and $\{1\}\{2\} \rightarrow \{x\}$ respectively) both had values of 0.011 ± 0.0325 , which is lower than the transfer atoms, but by less than an order of magnitude. Exactly what kind of biological process these modes correspond to is a promising area of future study. While every atom had particular pairs of neurons for which it was negative, at the aggregate level, every atom was, on average, greater than zero, including the higher-order measures, such as the double synergy ($\{12\} \rightarrow \{12\}$). These results show that spontaneous, on-going avalanche dynamics have a significant, element of consistently synergistic activity. For a complete set of correlations between all the atoms, see Supplementary Material Figure 9. We can also see that the information transfer atoms overall generally have the highest absolute values

To compare the results of the integrated information decomposition to a more established measure of systemic complexity, we compared the distribution of normalized Φ ID atoms to a measure of integrated information first proposed by Balduzzi & Tononi based on the difference between the total excess entropy and the sum of the two marginal excess entropies [52]:

$$\Phi^{WMS}(\mathbf{X}) = E(\mathbf{X}) - \sum_{i=0}^{|\mathbf{X}|} E(X_i) \quad (24)$$

Typically referred to as Φ^{WMS} (*WMS* indicating “whole-minus-sum”), it is a useful measure of non-trivial systemic integration (see [34] for a recent exploration of Φ^{WMS} in a Φ ID context). Φ^{WMS} has obvious parallels with the simple toy example of two predictors and a single target introduced in Section IA 1, with similar interpretations of the resulting sign (i.e. if $\Phi^{WMS} > 0$, then the system has synergistic dynamics only accessible when considering the whole as opposed to the independent parts). As with the histograms, we aggregated over all significant pairs of neurons in all the cultures, and correlated each ones Φ^{WMS} against each of the normalized Φ ID atoms. For visualization, see Figure 6.

Spearman correlation found that there was a very strong, negative correlation between Φ^{WMS} and the normalized information storage atoms ($\{x\} \rightarrow \{x\}$, $\rho = -0.8$, $p < 10^{-6}$, Bonferroni corrected). This is unsurprising, as information storage contributes to the marginal, within-element predictive information and contributes nothing to the higher-order interactions that comprise “integrated” information (consider the “disintegrated” toy model described above in Section III A). All other normalized Φ I atoms were positively correlated with Φ^{WMS} . The highest correlation was with the element-wise information transfer atoms ($\{x\} \rightarrow \{y\}$, $\rho = 0.57$, $p < 10^{-6}$, Bonferroni corrected). Since inter-element information transfer is a core element of systemic “integration”, and considering the overall high prevalence of bivariate transfer in the data (see Fig. 5), this result is unsurprising. As expected, the Φ I atoms containing higher-order synergies were all positively correlated with Φ^{WMS} , with the double-synergy term having one of the highest overall correlations ($\rho = 0.41$, $p < 10^{-6}$, Bonferroni corrected). This is consistent with the interpretation that Φ^{WMS} is an overall measure of total total systemic integration.

2. Local Φ ID Analysis

In addition to the average values of the integrated information atoms, the $I_{\tau sx}$ measure is localizable, allowing us to do a full, sixteen-atom decomposition for every moment in time, for every pair of neurons with significant excess entropy. We can leverage this property to perform a detailed analysis of the avalanches as temporally-extended objects qua themselves (rather than treating them as single units sampled from some heavy-tailed distribution). Across all pairs of neurons in all 31 cultures, we aggregated all avalanches of length $k > 4$, and if we observed at least 50 instances of avalanches of length k , we averaged them to create an “average profile.” Prior work with dissociated culture data has shown

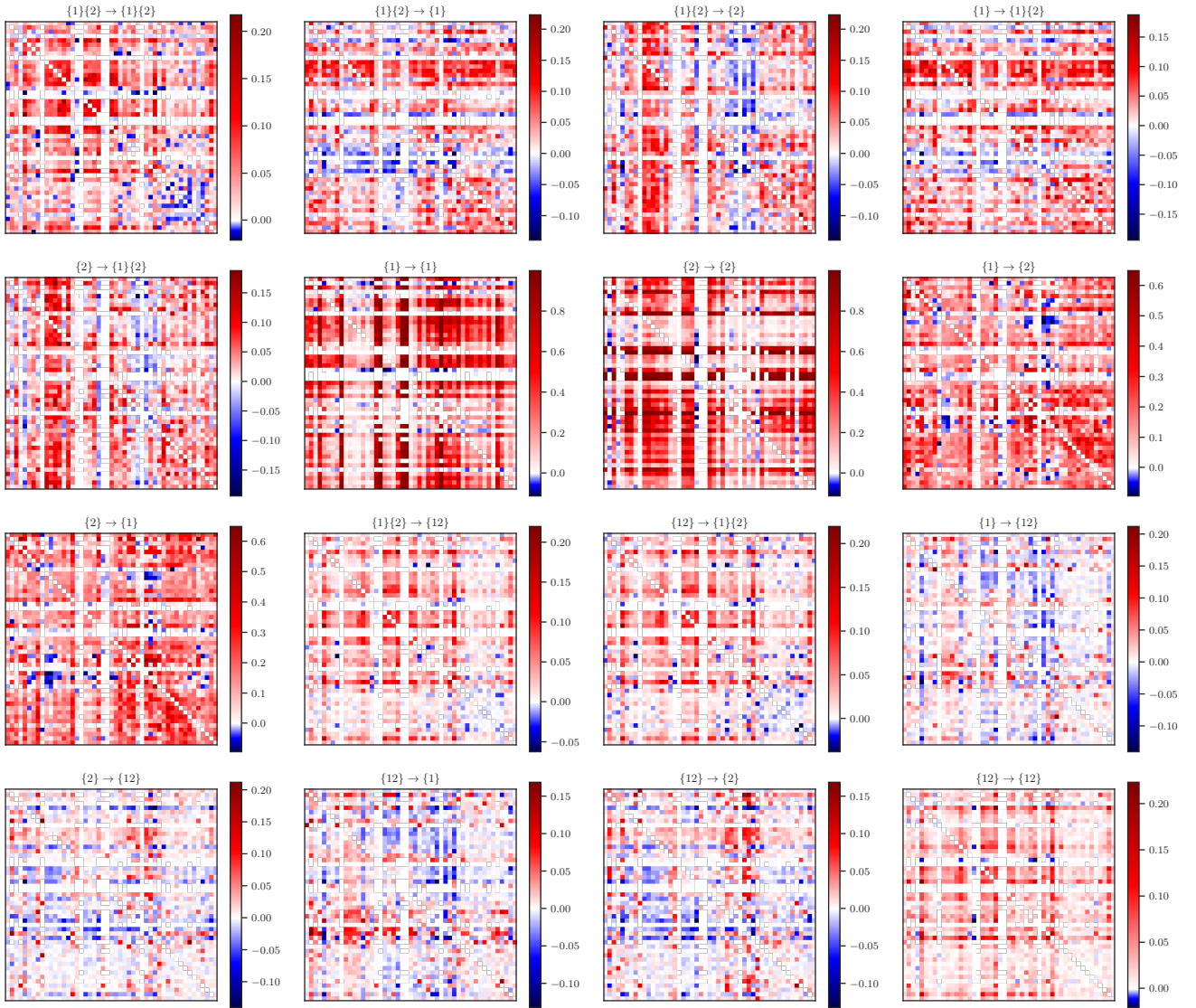


FIG. 4. **Visualized normalized Φ I matrices for a single culture.** For a single culture (in this case with approximately one hundred individual neurons), we can construct sixteen different pairwise matrices, each one corresponding to a Φ I atom. This contrasts with more well-known measures of functional and effective connectivity, which produce one matrix per system, reflecting a single “kind” of statistical relationship (be it functional connectivity, effective connectivity, etc). Integrated information decomposition, on the other hand, provides multiple “kinds” of relationship at once, allowing a far more complete picture of computational dynamics. Here, the value of each atom is normalized by the total excess entropy.

that avalanche profiles tend to be scaled versions of one another [12] (and references therein), showing a characteristic growth and then collapse of activity over the duration (for a visualization of the average avalanche profiles, see Figure 7, Upper Left). For every moment in the avalanches, we computed the excess entropy, and then performed the Φ ID using the local $i_{\tau_{sx}}$ to explore how the computational dynamics vary over the course of the avalanche. For a visualization of the profiles of the avalanches, the excess entropy, and all Φ I atoms, see Figure 7. Local Φ I atoms were not normalized, as the local excess entropy is a signed value, complicating the interpretation of a normalized value.

Upon visual inspection, it is clear that the various Φ I atoms have distinct profiles: for example, the profiles of the element-wise information storage and transfer atoms are characteristically similar to the excess entropy profiles, with rapid increases to a peak followed by a heavy tail. In contrast the double-synergy profile has a noisier shape, appearing to drop towards misinformation at the end of the avalanche. To explore these profile differences in more detail, we directly compared the spiking activity profiles to their associated informational profiles. We began by computing the *cumulative* profile for each avalanche: in the cumulative avalanche, every moment is given as the sum of all previous moments, including the

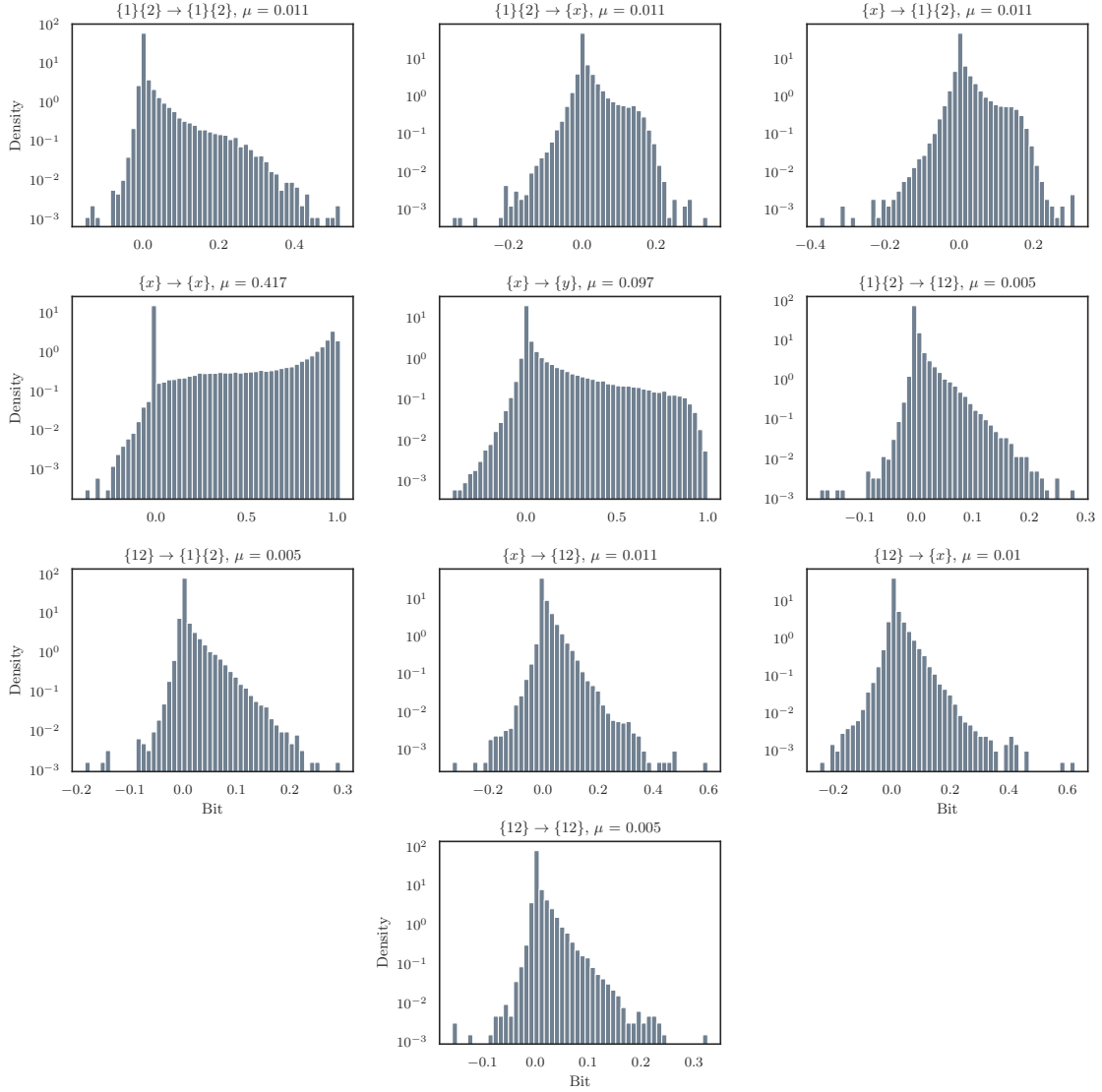


FIG. 5. **Histograms of the normalized ΦI atoms across all cultures.** The distributions of the normalized atoms show marked differences, depending on the particular kinds of information conversion occurring. For example, the element-wise information storage atom as the highest mean value and is considerably biased towards informative, positive relationships, while other measures display a more symmetric balance of informative and misinformative atoms (although all atoms displayed a bias towards informative relationships).

current one (analogous to a cumulative probability distribution). We then scaled each distribution by dividing it by the final, cumulative value, forcing all cumulative avalanches to terminate at 1. Finally, we filtered outlying cumulative avalanches that had unusually extreme deviations under the assumptions that they were contaminated by noise. By plotting the cumulative information atom avalanche distributions against the cumulative spiking avalanche distributions, we can assess how the growth and collapse of information atoms differs from the change in spiking dynamics (see Fig. 8). If the information atoms track the spiking activity perfectly, then the resulting curves will fall on the $y = x$ line. Deviations from the line of symmetry indicate a faster or slower ac-

cumulation of information than would be expected if it was perfectly correlated with spiking activity.

Visual inspection of the excess entropy cumulative profile reveals that avalanches are broadly-speaking informationally “front-heavy”, the local excess entropy climbs much faster than spikes accumulate (as seen by the curve climbing *above* the $y = x$ line), and has almost entirely “saturated” before halfway through the avalanche. When considering avalanches of differing lengths, this front-heaviness appears to become more pronounced for larger avalanches (for small avalanches of length between 4 and 10, the normalized cumulative distribution curves hug the line of symmetry much more closely). This suggests that, while all spiking avalanche profiles may be roughly

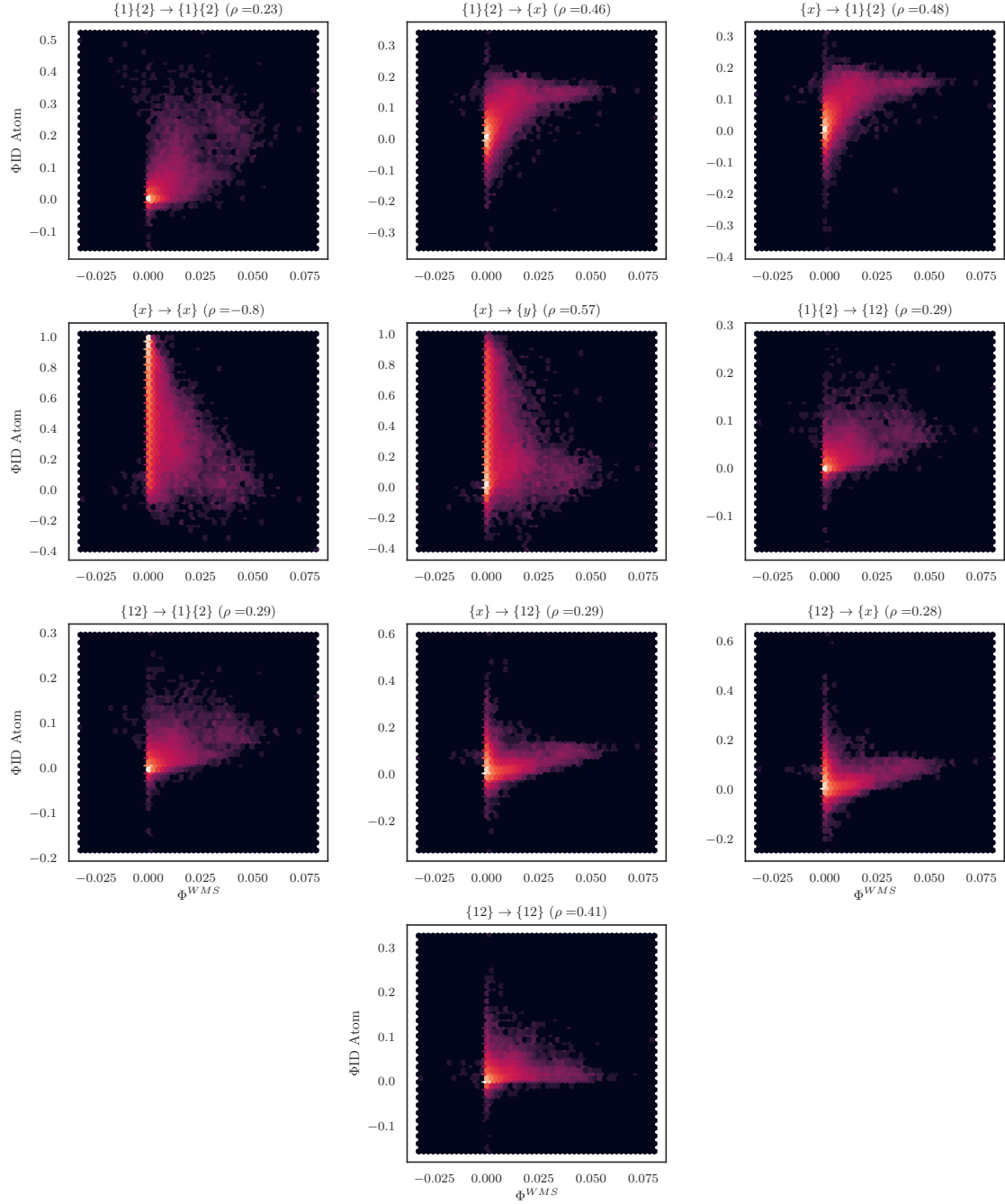


FIG. 6. Φ^{WMS} vs. **normalized ΦI Atoms**. We can see that the different normalized ΦI atoms have varying degrees of correlation with the Φ^{WMS} measure of integrated information [52]. While most are generally positively correlated, the element-level information-storage atom is a dramatic outlier, with a highly significant negative correlation of -0.8. We believe this occurs because a high degree of information storage in single elements means that the future of the whole is *mostly* predictable from the individual parts. The more individual elements disclose about their own future, the less “integrated” information in the system.

scaled versions of each-other, that scaling is not universal when it comes to information content: larger avalanches have different information profiles than smaller ones.

The pattern displayed by the cumulative excess entropy profile is broadly mirrored by the individual ΦI

atoms, although is the considerable variation between them. For example, the synergy-to-redundancy atom $\{12\} \rightarrow \{1\}\{2\}$ (and its mirror $\{1\}\{2\} \rightarrow \{12\}$) both hug the line of symmetry much more closely. In contrast, the the cumulative double redundancy profiles and

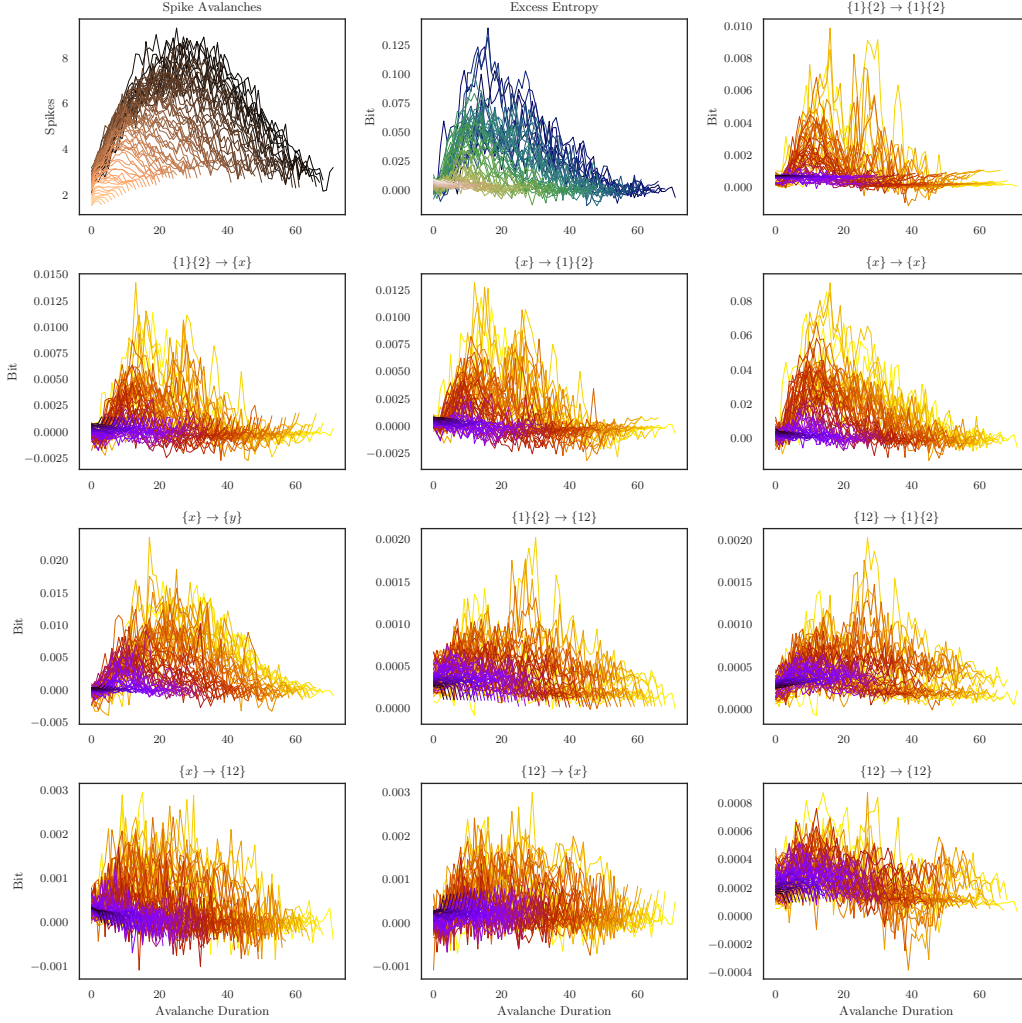


FIG. 7. **Average avalanche profile plots for spiking activity.** Each curve is the average profile for avalanches of duration $k > 4$ bins, if at least fifty avalanches of that duration were observed across the all thirty-one cultures. On the upper-leftmost square, we can see the average profile for raw spiking activity (copper colormap). In the uppermost center plot, we can see the average profile for the local excess entropy (blue-green colormap), and for the rest of the plots, the remaining Φ I atoms (violet-orange colormap). We can observe that different atoms have distinct characteristic profiles, some of which resemble the excess entropy more than others.

the cumulative information storage profiles track the cumulative excess entropy much more closely. Interestingly, the cumulative information copy and erasure profiles ($\{x\} \rightarrow \{1\}\{2\}$ and $\{1\}\{2\} \rightarrow \{x\}$) both achieve a maximum value before the end of the avalanche and then drop down, indicating a transition from informative to misinformative dynamics towards the end of the activity period. The cumulative double-synergy profile shows one of the most intriguing patterns: for large avalanches, it appears to have an S-shaped profile, initially climbing rapidly during the avalanche, before dropping across the line of symmetry. The significance of such a dynamic is unclear, and this is a finding well worth revisiting and replicating in a future data set.

Another interesting type of variability between atoms is how the profile changes with avalanche duration. In

the case of cumulative excess entropy, cumulative double-redundancy, and cumulative information storage, small avalanches reliably hug the line of symmetry and it is the larger avalanches that display interesting deviations. However, this is not the only pattern: for example the “downward causation” atom ($\{12\} \rightarrow \{x\}$) and the information erasure atoms both appear to display a kind of biphasic pattern: smaller avalanches (indicated by violet in Figure 8) run reliably *below* the line of symmetry, while large avalanches (indicated in orange) run above it.

From these results, we can see that the Φ ID framework, coupled with a localizable measure such as $I_{\tau sx}$ can provide a rich, novel approach to understanding ongoing neural activity and reveal patterns never before observed. For the purposes of this paper, we are restricting ourselves largely to qualitative analysis of local inte-

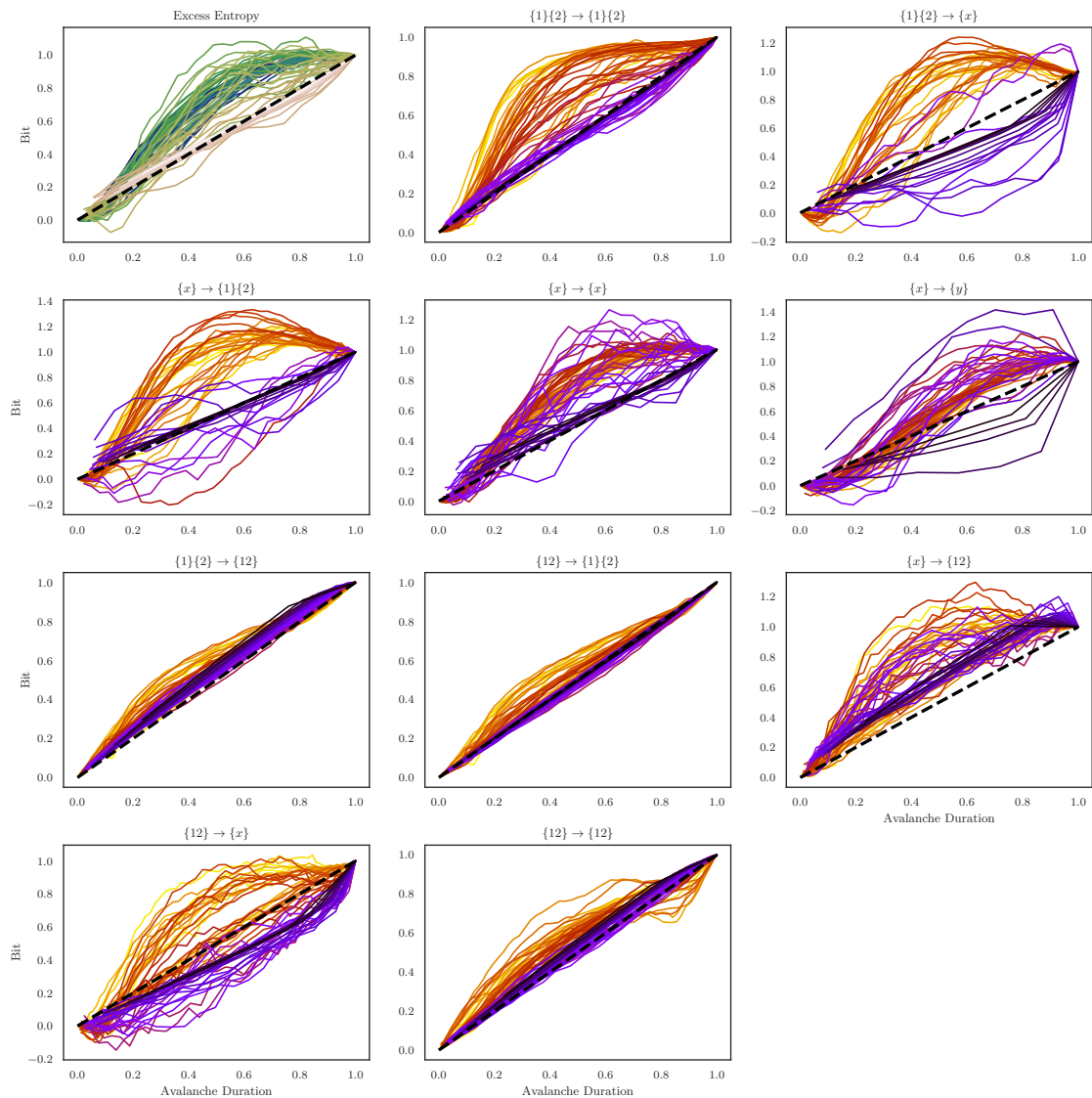


FIG. 8. **Cumulative information avalanche profiles plotted against cumulative spiking avalanche profiles.** These plots allow us to assess how the density of information atoms varies over the duration of the avalanche *relative to the spiking activity that defines the avalanche*. The black dotted line indicates the $y = x$ line of symmetry: if the information density of an atom hugs that line, then the profiles of both the information and the spiking activity are the same. We can see that, in many cases, the information profiles dramatically diverge from the line of symmetry, indicating that avalanches are “informationally front-leaded”, at least with respect to certain types of information integration.

grated information dynamics: the results presented here will require ample replication and much deeper study to determine their significance. In doing these analyses, we are confident that the field will witness unexpected, and fascinating discoveries both about the nervous system as well as about the structure of complex systems writ large.

IV. DISCUSSION

In this work, we have presented a novel information-theoretic measure, $I_{\tau sx}$, a generalization of the classic Shannon mutual information, that quantifies the re-

dundant information shared between multiple sources and multiple targets. $I_{\tau sx}$ is motivated by the recently proposed Integrated Information Decomposition [3, 8], which generalizes the classic single-target Partial Information Decomposition [7, 21] to sets of multiple interacted sources and targets. Like all information decompositions, the Φ ID is peculiar in that, while it reveals the *structure* of multivariate information, it lacks a crucial piece required to calculate numerical values from data. This is solved by providing $I_{\tau sx}$ as a redundancy function, with which the double redundancy lattice can be solved.

Here, the Φ ID framework is used to decompose the

excess entropy [1], which quantifies the total amount of statistical dependencies that constrains a systems evolution from past to future. Prior work [18] on using PID to decompose the excess entropy could reveal how the past states of individual components (and ensembles of components) constrain the future of the *whole* system, but provided no finer detail. Using the Φ ID, it is possible to understand how elements constrain their own futures, the future of other elements, groups of elements or the whole system in much finer resolution. To demonstrate the utility of the $I_{\tau_{sx}}$ measure in the Φ ID of the excess entropy, we first examined three small, completely specified toy models (each with it’s own enforced type of dynamic: integrated, disintegrated, or a mixture of the two) before moving on the empirical data recorded from dissociated cultures of rat cortex. We showed that both the average and local versions of $I_{\tau_{sx}}$ revealed rich information-dynamic structures in the data, including how different kinds of “neural computation” rise and fall as part of the bursty dynamics intrinsic to the nervous system. A significant benefit of the Φ ID framework is that it allows us to generalize different “kinds” of integration in a complex system such as the brain. Historically, information-theoretic approaches to integration have focused on single measures, such as integrated information theory’s eponymous measure [52]. The information decomposition framework, however reveals a multitude of different ways that groups of neurons compute their next state. Recent, promising work using fMRI data has started to relate various Φ I atoms (particular the synergistic atoms) to macro-scale brain dynamics [23], as well as different subcritical, critical, and supercritical dynamical regimes of various dynamical systems [34]. Given the wealth of data produced by modern neural recording methods, we are optimistic that there is a very wide world of possible applications of this framework.

While we have focused on the Φ ID framework as a means of decomposing the excess entropy of ongoing, spontaneous neural dynamics in dissociated cultures, in principle the framework could apply to any multi-source/target data set: the temporal dimension is not required. This opens up a wider range of applications of data analyses than is accessible to the classic PID - for example, Varley & Kaminsky recently used the PID to asses how varying social identities jointly information on single outcomes [55], however outcomes themselves are not independent and may contain interesting higher-order correlations within themselves: generalizing to a Φ ID framework may reveal many meaningful dependencies within social data, as well as many other fields where complex systems are studied.

Limitations

As currently formulated, the $I_{\tau_{sx}}$ function is only well-defined for discrete random variables, a feature that it inherits from the original I_{sx} measure [10]. Continuous

generalization of I_{sx} remains an area of active research [56] and it is assumed that a successful algorithm for I_{sx} will also work for $I_{\tau_{sx}}$. As it stands, the restriction to discrete random variables limits applicability. Prior work applying PID and Φ ID to naturally continuous data such as fMRI or cardiac rhythms has been done using measures of redundancy that are well-defined for Gaussian distributions [22, 23, 34], although these measures have their own limitations, such as lacking the intuitive interpretation, being non-localizable, or requiring arbitrary thresholds or optimizations.

Even in the event that a successful generalization of $I_{\tau_{sx}}$ is achieved, the PID and Φ ID frameworks struggle to scale gracefully for all but the smallest systems. In the case of the PID, the number of atoms in the lattice of a system of size k grows with the sequence of Dedekind numbers [7]: for a system with k elements, the associated lattice has $D(k) - 2$ atoms. Given how fast the Dedekind sequence grows, a complete decomposition of almost any interesting natural system (which can have thousands, or millions of components) is impossible. The Φ ID framework fares even worse, since there will be one temporal atom for every pair of partial information atoms in the associated PID lattice. The size of the Φ ID lattice then grows with the mind-boggling square of the Dedekind numbers: $(D(k) - 2)^2$ (a five element system will have a Φ ID lattice with 57,471,561 elements). Approximate heuristics such as the Φ^{WMS} measure, or more recently, the O-information [57, 58] have been proposed as efficient, if imprecise, tools for recognizing the presence of higher-order dependencies in dynamical data, however, there is still room for refinement. The final limitation is that the the structure of the Φ ID lattice, which allows for single sources to appear multiple times (e.g. $\{12\} \rightarrow \{x\}$ and $\{12\} \rightarrow \{12\}$ both incorporating the $\{12\}$ source) complicates the overall behavior of the redundancy functions. For example, the original I_{sx} function has certain, provable properties (such as the global non-negativity of it’s informative and misinformative components) that $I_{\tau_{sx}}$ cannot adopt, since the structure of the lattice is different. This strongly suggests that a return to the mathematical foundations of integrated information decomposition may be in order and new desiderata agreed on that may diverge from the single-target case.

V. CONCLUSIONS

In this work, we provide a redundancy function, $I_{\tau_{sx}}$ that can be used to decompose the total information that flows from the past to the future through the “channel” of a multi-element, dynamic system. This framework, when applied to neural data reveals a rich repertoire of complex computational dynamics that can be temporally localized to the scale of individual moments in time. Based on the fundamental logic of information as exclusions of probability mass, $I_{\tau_{sx}}$ generalizes the classic Shannon entropy and we anticipate that the work presented here will open

new doors both in the specific fields of neuroscience as well as in complex systems science more generally.

ACKNOWLEDGEMENTS

T.F.V is supported by NSF-NRT grant 1735095, Interdisciplinary Training in Complex Networks and Systems

at Indiana University Bloomington. I would like to thank Dr. John Beggs & Dr. Olaf Sporns for mentorship and feedback on this project. I would also like to thank Dr. Abolfazl Alipour and Mr. Leandro Fosque for providing the dissociated culture data.

-
- [1] James P. Crutchfield and David P. Feldman. Regularities unseen, randomness observed: Levels of entropy convergence. *Chaos: An Interdisciplinary Journal of Nonlinear Science*, 13(1):25–54, January 2003. Number: 1 Publisher: American Institute of Physics.
- [2] Ryan G. James, Christopher J. Ellison, and James P. Crutchfield. Anatomy of a bit: Information in a time series observation. *Chaos: An Interdisciplinary Journal of Nonlinear Science*, 21(3):037109, September 2011. Publisher: American Institute of Physics.
- [3] Pedro A. M. Mediano, Fernando E. Rosas, Andrea I. Luppi, Robin L. Carhart-Harris, Daniel Bor, Anil K. Seth, and Adam B. Barrett. Towards an extended taxonomy of information dynamics via Integrated Information Decomposition. *arXiv:2109.13186 [physics, q-bio]*, September 2021. arXiv: 2109.13186.
- [4] Øistein Schmidt Galaaen. *The Disturbing Matter of Downward Causation*. PhD Thesis, University of Oslo, 2006.
- [5] Paul C. W. Davies. The Physics of Downward Causation. In *The Re-Emergence of Emergence*. Oxford University Press, Oxford, 2008.
- [6] Paul L. Williams and Randall D. Beer. Non-negative Decomposition of Multivariate Information. *arXiv:1004.2515 [math-ph, physics:physics, q-bio]*, April 2010. arXiv: 1004.2515.
- [7] A. J. Gutknecht, M. Wibral, and A. Makkeh. Bits and pieces: understanding information decomposition from part-whole relationships and formal logic. *Proceedings of the Royal Society A: Mathematical, Physical and Engineering Sciences*, 477(2251):20210110, July 2021. Publisher: Royal Society.
- [8] Pedro A. M. Mediano, Fernando Rosas, Robin L. Carhart-Harris, Anil K. Seth, and Adam B. Barrett. Beyond integrated information: A taxonomy of information dynamics phenomena. *arXiv:1909.02297 [physics, q-bio]*, September 2019. arXiv: 1909.02297.
- [9] Fernando E. Rosas, Pedro A. M. Mediano, Henrik J. Jensen, Anil K. Seth, Adam B. Barrett, Robin L. Carhart-Harris, and Daniel Bor. Reconciling emergences: An information-theoretic approach to identify causal emergence in multivariate data. *PLOS Computational Biology*, 16(12):e1008289, December 2020. Number: 12 Publisher: Public Library of Science.
- [10] Abdullah Makkeh, Aaron J. Gutknecht, and Michael Wibral. Introducing a differentiable measure of pointwise shared information. *Physical Review E*, 103(3):032149, March 2021. Publisher: American Physical Society.
- [11] Chadwick M. Hales, John D. Rolston, and Steve M. Potter. How to culture, record and stimulate neuronal networks on micro-electrode arrays (MEAs). *Journal of Visualized Experiments: JoVE*, (39):2056, May 2010.
- [12] Nicholas M. Timme, Najja J. Marshall, Nicholas Bennett, Monica Ripp, Edward Lautzenhiser, and John M. Beggs. Criticality Maximizes Complexity in Neural Tissue. *Frontiers in Physiology*, 7, 2016.
- [13] Nils Bertschinger, Johannes Rauh, Eckehard Olbrich, and Jürgen Jost. Shared Information – New Insights and Problems in Decomposing Information in Complex Systems. *arXiv:1210.5902 [cs, math]*, pages 251–269, 2013. arXiv: 1210.5902.
- [14] Nils Bertschinger, Johannes Rauh, Eckehard Olbrich, Jürgen Jost, and Nihat Ay. Quantifying Unique Information. *Entropy*, 16(4):2161–2183, April 2014. Number: 4 Publisher: Multidisciplinary Digital Publishing Institute.
- [15] Ryan G. James, Jeffrey Emenheiser, and James P. Crutchfield. Unique Information and Secret Key Agreement. *Entropy*, 21(1):12, January 2019. Number: 1 Publisher: Multidisciplinary Digital Publishing Institute.
- [16] Rick Quax, Omri Har-Shemesh, and Peter M. A. Sloot. Quantifying Synergistic Information Using Intermediate Stochastic Variables. *Entropy*, 19(2):85, February 2017. Number: 2 Publisher: Multidisciplinary Digital Publishing Institute.
- [17] Fernando E. Rosas, Pedro A. M. Mediano, Borzoo Rasouli, and Adam B. Barrett. An operational information decomposition via synergistic disclosure. *Journal of Physics A: Mathematical and Theoretical*, 53(48):485001, November 2020. Publisher: IOP Publishing.
- [18] Thomas Varley and Erik Hoel. Emergence as the conversion of information: A unifying theory. *arXiv:2104.13368 [cs, math]*, April 2021. arXiv: 2104.13368.
- [19] Joseph T. Lizier. *The Local Information Dynamics of Distributed Computation in Complex Systems*. Springer Theses. Springer Berlin Heidelberg, Berlin, Heidelberg, 2013.
- [20] Terry Bossomaier, Lionel Barnett, Michael Harré, and Joseph T. Lizier. *An Introduction to Transfer Entropy: Information Flow in Complex Systems*. Springer, November 2016. Google-Books-ID: p8eADQAAQBAJ.
- [21] Paul L. Williams and Randall D. Beer. Generalized Measures of Information Transfer. *arXiv:1102.1507 [physics]*, February 2011. arXiv: 1102.1507.
- [22] Andrea I. Luppi, Pedro A. M. Mediano, Fernando E. Rosas, Judith Allanson, John D. Pickard, Robin L. Carhart-Harris, Guy B. Williams, Michael M. Craig, Paola Finoaia, Adrian M. Owen, Lorina Naci, David K. Menon, Daniel Bor, and Emmanuel A. Stamatakis. A Synergistic Workspace for Human Consciousness

- Revealed by Integrated Information Decomposition. *bioRxiv*, page 2020.11.25.398081, November 2020. Publisher: Cold Spring Harbor Laboratory Section: New Results.
- [23] Andrea I. Luppi, Pedro A. M. Mediano, Fernando E. Rosas, Negin Holland, Tim D. Fryer, John T. O'Brien, James B. Rowe, David K. Menon, Daniel Bor, and Emmanuel A. Stamatakis. A synergistic core for human brain evolution and cognition. *bioRxiv*, page 2020.09.22.308981, September 2020. Publisher: Cold Spring Harbor Laboratory Section: New Results.
- [24] Malte Harder, Christoph Salge, and Daniel Polani. Bivariate measure of redundant information. *Physical Review E, Statistical, Nonlinear, and Soft Matter Physics*, 87(1):012130, January 2013.
- [25] Virgil Griffith, Edwin K. P. Chong, Ryan G. James, Christopher J. Ellison, and James P. Crutchfield. Intersection Information Based on Common Randomness. *Entropy*, 16(4):1985–2000, April 2014. Number: 4 Publisher: Multidisciplinary Digital Publishing Institute.
- [26] Virgil Griffith and Christof Koch. Quantifying synergistic mutual information. *arXiv:1205.4265 [cs, math, q-bio]*, March 2014. arXiv: 1205.4265.
- [27] Eckehard Olbrich, Nils Bertschinger, and Johannes Rauh. Information Decomposition and Synergy. *Entropy*, 17(5):3501–3517, May 2015. Number: 5 Publisher: Multidisciplinary Digital Publishing Institute.
- [28] Adam B. Barrett. Exploration of synergistic and redundant information sharing in static and dynamical Gaussian systems. *Physical Review E*, 91(5):052802, May 2015. Publisher: American Physical Society.
- [29] Allison E. Goodwell and Praveen Kumar. Temporal information partitioning: Characterizing synergy, uniqueness, and redundancy in interacting environmental variables. *Water Resources Research*, 53(7):5920–5942, 2017.
- [30] Robin A. A. Ince. Measuring Multivariate Redundant Information with Pointwise Common Change in Surprisal. *Entropy*, 19(7):318, July 2017. Number: 7 Publisher: Multidisciplinary Digital Publishing Institute.
- [31] Conor Finn and Joseph T. Lizier. Pointwise Partial Information Decomposition Using the Specificity and Ambiguity Lattices. *Entropy*, 20(4):297, April 2018. Number: 4 Publisher: Multidisciplinary Digital Publishing Institute.
- [32] Nihat Ay, Daniel Polani, and Nathaniel Virgo. Information Decomposition based on Cooperative Game Theory. *arXiv:1910.05979 [cs, math]*, October 2019. arXiv: 1910.05979.
- [33] Artemy Kolchinsky. A novel approach to multivariate redundancy and synergy. *arXiv:1908.08642 [cs, math, q-bio, stat]*, August 2019. arXiv: 1908.08642.
- [34] Pedro A. M. Mediano, Fernando E. Rosas, Juan Carlos Farah, Murray Shanahan, Daniel Bor, and Adam B. Barrett. Integrated information as a common signature of dynamical and information-processing complexity. *Chaos: An Interdisciplinary Journal of Nonlinear Science*, 32(1):013115, January 2022. Publisher: American Institute of Physics.
- [35] Conor Finn and Joseph T. Lizier. Probability Mass Exclusions and the Directed Components of Mutual Information. *Entropy*, 20(11):826, November 2018. Number: 11 Publisher: Multidisciplinary Digital Publishing Institute.
- [36] Woodrow L. Shew, Hongdian Yang, Shan Yu, Rajarshi Roy, and Dietmar Plenz. Information Capacity and Transmission Are Maximized in Balanced Cortical Networks with Neuronal Avalanches. *Journal of Neuroscience*, 31(1):55–63, January 2011. Number: 1.
- [37] Samantha P. Faber, Nicholas M. Timme, John M. Beggs, and Ehren L. Newman. Computation is concentrated in rich clubs of local cortical networks. *Network Neuroscience*, 3(2):1–21, September 2018.
- [38] Samantha P. Sherrill, Nicholas M. Timme, John M. Beggs, and Ehren L. Newman. Correlated activity favors synergistic processing in local cortical networks in vitro at synaptically relevant timescales. *Network Neuroscience*, 4(3):678–697, July 2020.
- [39] Samantha P. Sherrill, Nicholas M. Timme, John M. Beggs, and Ehren L. Newman. Partial information decomposition reveals that synergistic neural integration is greater downstream of recurrent information flow in organotypic cortical cultures. *PLOS Computational Biology*, 17(7):e1009196, July 2021. Publisher: Public Library of Science.
- [40] Michael Wibral, Conor Finn, Patricia Wollstadt, Joseph T. Lizier, and Viola Priesemann. Quantifying Information Modification in Developing Neural Networks via Partial Information Decomposition. *Entropy*, 19(9):494, September 2017. Number: 9 Publisher: Multidisciplinary Digital Publishing Institute.
- [41] Priscila C. Antonello, Thomas F. Varley, John Beggs, Marimelia Porcionatto, Olaf Sporns, and Jean Faber. Self-organization of in vitro neuronal assemblies drives to complex network topology. Technical report, bioRxiv, November 2021. Section: New Results Type: article.
- [42] David P. Shorten, Viola Priesemann, Michael Wibral, and Joseph T. Lizier. Early lock-in of structured and specialised information flows during neural development. *bioRxiv*, page 2021.06.29.450432, June 2021. Publisher: Cold Spring Harbor Laboratory Section: New Results.
- [43] Shinya Ito, Fang-Chin Yeh, Emma Hiolski, Przemyslaw Rydygier, Deborah E. Gunning, Pawel Hottowy, Nicholas Timme, Alan M. Litke, and John M. Beggs. Large-Scale, High-Resolution Multielectrode-Array Recording Depicts Functional Network Differences of Cortical and Hippocampal Cultures. *PLOS ONE*, 9(8):e105324, August 2014. Number: 8.
- [44] Sunny Nigam, Masanori Shimono, Shinya Ito, Fang-Chin Yeh, Nicholas Timme, Maxym Myroshnychenko, Christopher C. Laphis, Zachary Tosi, Pawel Hottowy, Wesley C. Smith, Sotiris C. Masmanidis, Alan M. Litke, Olaf Sporns, and John M. Beggs. Rich-Club Organization in Effective Connectivity among Cortical Neurons. *Journal of Neuroscience*, 36(3):670–684, January 2016. Publisher: Society for Neuroscience Section: Articles.
- [45] Nicholas Timme, Shinya Ito, Maxym Myroshnychenko, Fang-Chin Yeh, Emma Hiolski, Pawel Hottowy, and John M. Beggs. Multiplex Networks of Cortical and Hippocampal Neurons Revealed at Different Timescales. *PLOS ONE*, 9(12):e115764, December 2014. Publisher: Public Library of Science.
- [46] Felix Goetze and Pik-Yin Lai. Reconstructing positive and negative couplings in Ising spin networks by sorted local transfer entropy. *Physical Review E*, 100(1):012121, July 2019. Publisher: American Physical Society.
- [47] John M. Beggs and Nicholas Timme. Being Critical of Criticality in the Brain. *Frontiers in Physiology*, 3, 2012.

- [48] John M. Beggs. The Critically Tuned Cortex. *Neuron*, 104(4):623–624, November 2019. Number: 4.
- [49] Alain Destexhe and Jonathan D. Touboul. Is There Sufficient Evidence for Criticality in Cortical Systems? *eNeuro*, 8(2), March 2021. Publisher: Society for Neuroscience Section: Commentary.
- [50] John M. Beggs and Dietmar Plenz. Neuronal Avalanches in Neocortical Circuits. *Journal of Neuroscience*, 23(35):11167–11177, December 2003. Number: 35.
- [51] Thomas Varley, Olaf Sporns, Aina Puce, and John Beggs. Differential effects of propofol and ketamine on critical brain dynamics. *PLOS Computational Biology*, 16(12):e1008418, December 2020. Number: 12 Publisher: Public Library of Science.
- [52] David Balduzzi and Giulio Tononi. Integrated information in discrete dynamical systems: motivation and theoretical framework. *PLoS computational biology*, 4(6):e1000091, June 2008.
- [53] Michael Wibral, Joseph Lizier, Sebastian Vögler, Viola Priesemann, and Ralf Galuske. Local active information storage as a tool to understand distributed neural information processing. *Frontiers in Neuroinformatics*, 8, 2014. Publisher: Frontiers.
- [54] Thomas Varley, Olaf Sporns, Hansjorg Scherberger, and Benjamin Dann. Information dynamics in neuronal networks of macaque cerebral cortex reflect cognitive state and behavior. Technical report, September 2021. Company: Cold Spring Harbor Laboratory Distributor: Cold Spring Harbor Laboratory Label: Cold Spring Harbor Laboratory Section: New Results Type: article.
- [55] Thomas F. Varley and Patrick Kaminski. Intersectional synergies: untangling irreducible effects of intersecting identities via information decomposition. *arXiv:2106.10338 [physics, stat]*, October 2021. arXiv: 2106.10338.
- [56] Kyle Schick-Poland, Abdullah Makkeh, Aaron J. Gutknecht, Patricia Wollstadt, Anja Sturm, and Michael Wibral. A partial information decomposition for discrete and continuous variables. *arXiv:2106.12393 [cs, math]*, June 2021. arXiv: 2106.12393.
- [57] Fernando Rosas, Pedro A. M. Mediano, Michael Gastpar, and Henrik J. Jensen. Quantifying High-order Interdependencies via Multivariate Extensions of the Mutual Information. *Physical Review E*, 100(3):032305, September 2019. Number: 3 arXiv: 1902.11239.
- [58] Sebastiano Stramaglia, Tomas Scagliarini, Bryan C. Daniels, and Daniele Marinazzo. Quantifying Dynamical High-Order Interdependencies From the O-Information: An Application to Neural Spiking Dynamics. *Frontiers in Physiology*, 11, 2021. Publisher: Frontiers.
- [59] R. Quiñero, Z. Nadasdy, and Y. Ben-Shaul. Unsupervised Spike Detection and Sorting with Wavelets and Superparamagnetic Clustering. *Neural Computation*, 16(8):1661–1687, August 2004.
- [60] David R. Brillinger. Some data analyses using mutual information. *Brazilian Journal of Probability and Statistics*, 18(2):163–182, 2004. Publisher: [Brazilian Statistical Association, Institute of Mathematical Statistics].
- [61] Philip E. Cheng, Jiun W. Liou, Michelle Liou, and John AD Aston. Data information in contingency tables: a fallacy of hierarchical loglinear models. *Journal of Data Science*, 4(4):387–398, 2006.
- [62] Joseph T. Lizier. JIDT: An Information-Theoretic Toolkit for Studying the Dynamics of Complex Systems. *Frontiers in Robotics and AI*, 1, 2014. Publisher: Frontiers.
- [63] Patricia Wollstadt, Joseph T. Lizier, Raul Vicente, Conor Finn, Mario Martinez-Zarzuela, Pedro Mediano, Leonardo Novelli, and Michael Wibral. IDTxl: The Information Dynamics Toolkit xl: a Python package for the efficient analysis of multivariate information dynamics in networks. *Journal of Open Source Software*, 4(34):1081, February 2019. Number: 34.

MATERIALS & METHODS

Dissociated Culture Preparation & Recording

The details of the general process for the preparation of dissociated cultures can be found in [11]. Here we summarize the specific methodologies detailed in [12], who first introduced this dataset. Pregnant Sprague-Dawley rats (Harlan Laboratories) on Day 18 of gestation were euthanized via CO₂ and the embryos removed. Embryonic hippocampal tissue was resected and dissociated en masse before being plated on a Multichannel Systems 60 electrode arrays (8 × 8, 200 μm electrode spacing, 30 μm electrode diameter). Spontaneous activity was recording at 20,000 Hz for approximately 1 hour (for this analysis, all recordings longer than 60 minutes were terminated at that point). The resulting spikes were sorted with the wave_Clus algorithm [59] to infer individual neurons. Following spike sorting, the data were rebinned to 3ms bins (approximating the average inter-spike interval for the set of all 31 the recordings).

Mutual Information Calculation & Significance Testing

For every pair of neurons in a given culture, we calculated the mutual information between those two nodes at time t and the same two nodes at time $t + 1$:

$$I(\mathbf{X}_t; \mathbf{X}_{t+1}) = H(\mathbf{X}_t) + H(\mathbf{X}_{t+1}) - H(\mathbf{X}_t, \mathbf{X}_{t+1}) \quad (25)$$

Where $H(\cdot)$ is the classical Shannon entropy function. We significance tested each pair against the analytic null distribution for discrete random variables with finite alphabets [60, 61], with an $\alpha = 10^{-6}$, followed by Bonferroni correction. The analytic null estimator allows for very efficient estimation of p-values, requiring minimal compute time (and reducing the associated carbon costs associated with time-intensive high-performance computing). We used the implementation provided by JIDT

[62], accessed via the IDTxl package [63] for its efficient Python interface.

Constructing Toy Boolean Networks

For the integrated and disintegrated example systems, the transition probabilities were worked out by hand from first principles. The heterogenous system was constructed based on the details provided in [18]. Briefly, a 4×4 transition probability matrix was initialized, and every entry M_{ij} was drawn from a normal distribution with unit mean and variance. The absolute value was taken, and the out-going probabilities normalized to define a discrete probability distribution.

Excluding Noisy Cumulative Avalanche Profiles

To remove information avalanche profiles excessively contaminated by noise, we excluded any cumulative avalanche profiles that had an excursion of more than 1 bit away from the $y = x$ line or a total length greater than 2 bit. With these thresholds, we excluded on average 7.5 ± 8.18 avalanches for each ΦI atom. To see the full set of unfiltered cumulative avalanche plots, see Supplemental Figure 10

Data and Code Availability

The raw spiking data is available on the CRCNS neuroscience data-sharing portal (<https://crcns.org/data-sets/hc/hc-8>). Data was binned to 3 ms bins and a 60-minute cut-off was applied to any recordings longer than one hour. All Python code is available upon request, and will be released publicly upon formal publication of this manuscript.

SUPPLEMENTAL FIGURES

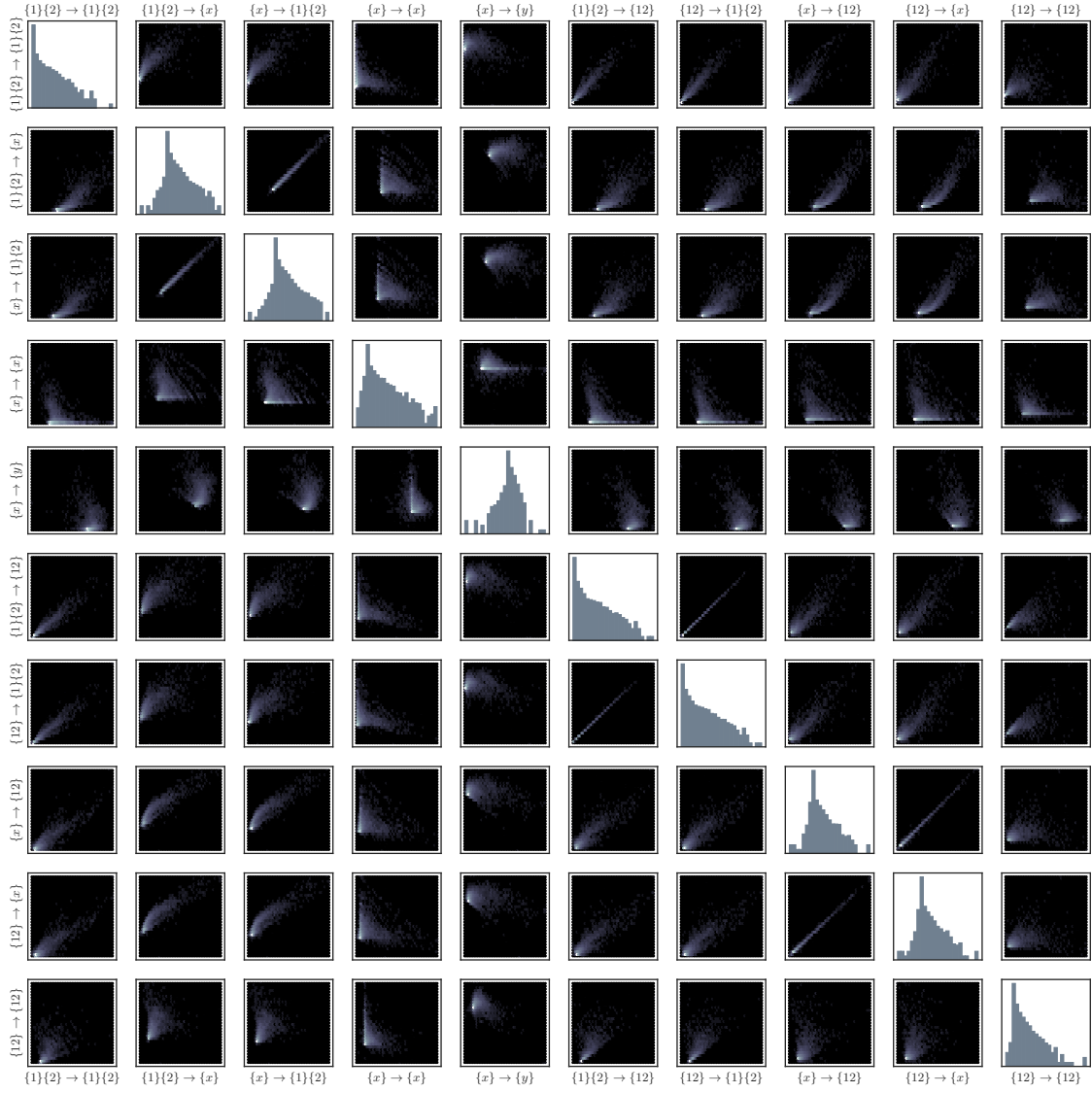


FIG. 9. All pairwise correlations between normalized $\Phi\mathbf{I}$ atoms. Represented as two-dimensional log-probability density hexagonal histograms. The middle diagonal replicates the histograms seen in Figure 5. We can see that the correlations between various atoms are complex and not always trivial, or linear.

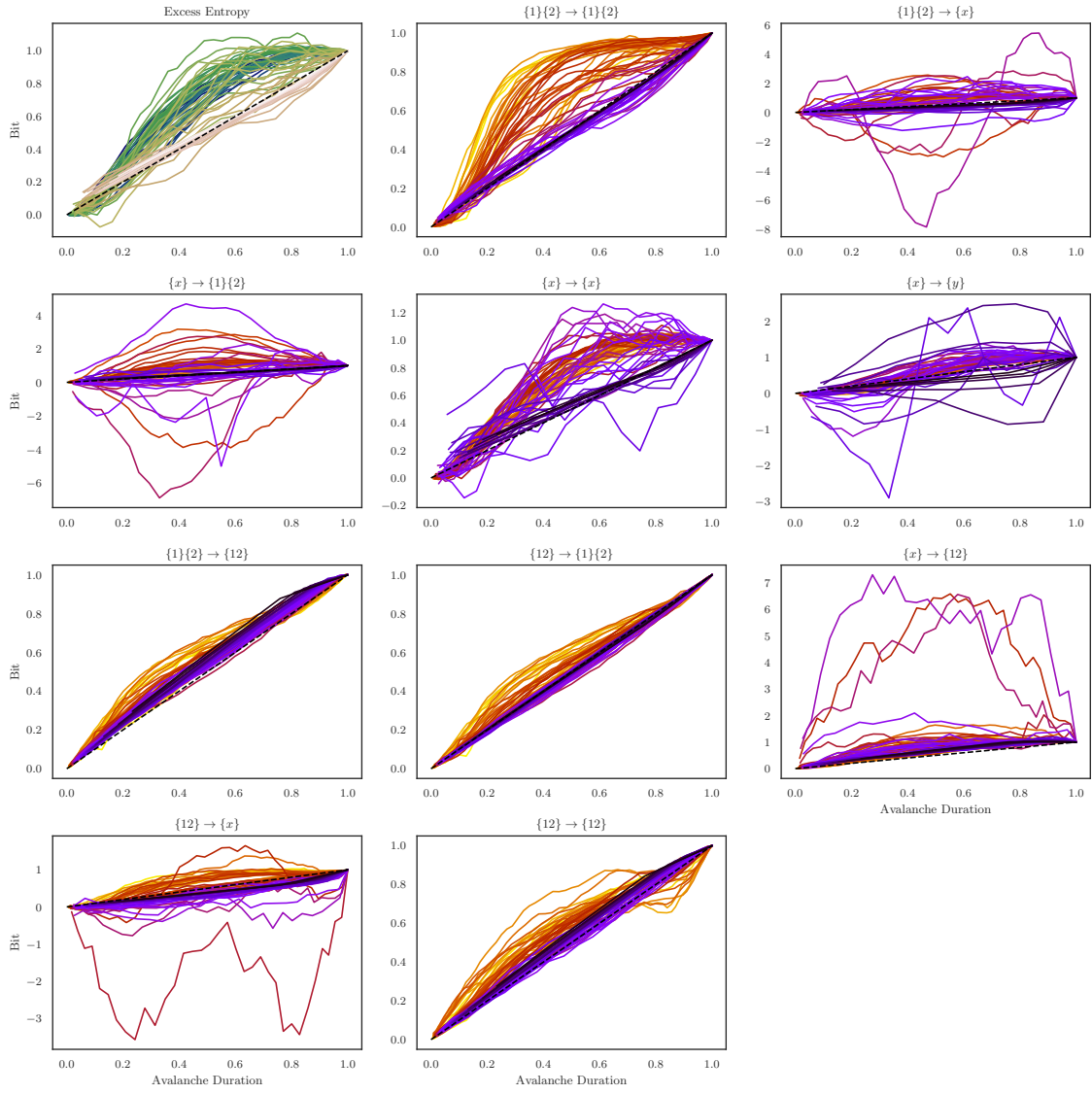


FIG. 10. All cumulative avalanche plots without the filters. Visual comparison with Figure 8 shows that the overall pattern can still be discerned despite the very noisy avalanches.